NTNU

Norwegian University of
Science and Technology

Electrochemical reactions of Carboxylic Acids and product identification

Ragnhild Helene Gulbrandsen

Chemical Engineering and Biotechnology
Submission date: June 2011
Supervisor: Frode Seland, IMTE
Co-supervisor: Svein Sunde, IMTE
Børre T. Børresen, Statoil

Norwegian University of Science and Technology
Department of Materials Science and Engineering

Preface

This master thesis work was carried out at the Department of Materials Science and Engineering, at the Norwegian University of Science and Technology, as a part of my masters degree in Industrial chemistry and biotechnology with specialization in Materials Chemistry and Energy technology.

Several people were involved during this project and to whom I would like to direct my appreciation here.

I wish to thank my main supervisor Associate professor Frode Seland for vital guidance and support throughout this year, especially during the finishing stage, and my co-supervisors Dr. Børre Børresen (Statoil) and Professor Svein Sunde for their involvement.

A special thank you to Luis Colmenares (SINTEF Materials and Chemistry) for his contribution to the IR related portion of this master thesis work, involving design, build, experimental work and troubleshooting, as well as finding relevant literature.

Thanks to the workshop and glassworker at the Faculty of Natural Sciences and Technology for manufacturing the pieces for the IR setup.

Thanks to PhD student Malin Sletnes for help with booking of the IR spectrometer, and Professor Martin Ystenes for technical information on it. And thanks to PhD student Lars Erik Owe for his contribution during troubleshooting of the electrochemical setup early in February.

Thanks to fellow master student Steffen Bugge at the Department of Chemistry, Section for Organic Chemistry, for input on proposed mechanism for oxidation of carboxylic acids consisting of more than one carbon atom.

Last, but not least, thanks to my fiancé for his patient support whenever I've been stressed out or worked long hours. And thanks to my family for always believing in me.

– – – – – – – – – – – – – – – – – – –

Ragnhild Helene Gulbrandsen, Trondheim June 22, 2011

Abstract

The research effort on renewable energy sources and biofuels have increased significantly during recent years, due to dwindling reserves of fossil fuels and the increased attention on climate changes presumably caused by carbon dioxide emissions. Four alcohols and four carbxoxylic acids, namely methanol, ethanol, 1-propanol, 1-butanol, formic acid, acetic acid, propionic acid and butyric acid were studied in this masters thesis by electrochemical means with the aim of demonstrating any electrochemical reduction of carboxylic acids. Oxidation of the alcohols happened more readily than oxidation of the acids (hence peak current density was significantly higher) which contained at least one C-C bond. Looking closer at the lower potential end of the voltammetry experiments (H_{UPD} region), a dissimilarity was observed in particular between the base electrolyte and high concentration of longer chained acids (propionic and butyric acid). Furthermore, long-term experiments of holding a constant potential in the H_{UPD}/HER region gave rise to a new oxidation peak in the voltammogram, as well as a small reduction peak at about the same potential (0.5 V). This new characteristic may indicate the possible existence of a slow process in this low potential region. On the other hand, short term experiments gave no indications of production of anything other than hydrogen in the hydrogen evolution region. In most cases a slightly less negative current density was observed, probably due to some sort of blocking of the active sites by carbonaceous species. The existence of an enhanced reduction current in the H_{UPD} region called for methods to detect adsorbed intermediates at the surface and soluble byproducts. A setup for external reflection mode ATR-FTIR spectroscopy was employed in this work. In this project oxidation of CO was used to justify the setup and the glass cell. A small signal corresponding to adsorbed CO was indeed observed indicating that the setup is working as intended, although further work is needed to increase signal strength, improve quality and reproducibility. We can not conclude or exclude whether the interesting current characteristics occurring in the hydrogen underpotential deposition region (especially for 1 M propionic and butyric acid), and during the long-term experiment for butyric acid is indeed electrochemical reduction. Further work concerning product analysis is highly desired.

Symbols and Abbreviations

ATR Attenuated Total Reflectance

CE Counter Electrode

CV Cyclic Voltammogram

DEMS Differential Electrochemical Mass Spectrometry

E_{lower} Negative turn-round potential [V vs. RHE]

E_{upper} Positive turn-round potential [V vs. RHE]

FTIR Fourier Transform Infrared Spectroscopy

HER Hydrogen Evolution Reaction

H_{UPD} Hydrogen underpotential deposition region

LSV Linear Sweep Voltammogram

OCP Open Circuit Potential [V vs. RHE]

RDE Rotating disk electrode

RHE Reversible Hydrogen Electrode

WE Working Electrode

θ_i Surface coverage of species i

Contents

List of Figures

List of Tables

1 Introduction

The research effort on renewable energy sources and biofuels have increased significantly during recent years, due to dwindling reserves of fossil fuels and the increased attention on climate changes presumably caused by carbon dioxide emissions. For instance, the activity in the field of hydrocarbon fuel cells has increased [1], and a carbon-based analogy to the hydrogen economy has been proposed for methanol among other small organic molecules [2].

Statoil has, through their research on second generation biofuels, developed a process in which bacteria convert sugars from decomposed cellulose into butyric acid and small amounts of butanol. The energy content of the butanol molecule is higher than for both methanol and ethanol, and thus have the potential to be a good liquid fuel. Another advantage of butanol over ethanol is that commercial gasoline motors can run on butanol without expensive modifications [3]. These qualities, among others, make butanol a better alternative as a biofuel than ethanol. Hence, it is desirable to convert the butyric acid into butanol as written by Atsumi et al. [4].

Traditionally, only oxidation have been studied for small organic molecules, which occur within the potential stability region of H_2O. The thought of reducing organic compounds electrochemically on the other hand is relatively new, thus little literature is available on the subject. The common way of reducing organic compounds today is by chemical reduction with hydrogen gas or other highly reactive reducing agents [5], which is a complex and expensive process, and less safe on an industrial scale than electrolysis in aqueous solution.

Four primary alcohols and four carboxylic acids, namely methanol, ethanol, 1-propanol, 1-butanol, formic acid, acetic acid, propionic acid and butyric acid were studied in this masters thesis utilizing electrochemical techniques, such as sweep voltammetry, potential steps and rotating disk electrode.

The goal of the work initiated in this thesis work, was to investigate whether convertion of butyric acid into butanol can be achieved through electrochemical reduction in aqueous solution and to unravel the possible electrochemical mechanism of the electrode processes. It is expected that the selectivity will depend on the potential and electrode material as written by Hori et al. [6]. In this thesis work, the focus has been split into two parts, one that looks into the reduction and oxidation of the various organic compounds at a smooth platinum electrode, and a second one that deals with well known oxidation processes (like CO) and method development. Knowledge of the lighter compounds kinetics may yield important information of the reactivity of the longer C-chained molecules in the electrochemical system, and map possible fingerprints for reaction intermediates or products. Qualitative statements are drawn with respect to the response from longer C-chained alcohols and carboxylic acids, as compared to the primary ones.

The objective of the IR spectroscopy related work was to initiate activity in this field so in the long term more detailed information on these processes can be obtained. The possibility of identifying both adsorbed and dissolved species make it a powerful tool for studying mechanisms in electrocatalysis, especially in combination with DEMS as employed by Heinen et al. [7, 8, 9, 10], among others [11, 12].

2 Theory and background

2.1 Reduction processes

Today, organic compounds are most commonly reduced chemically with H_2(g) or various other reducing agents. An aldehyde is reduced to a primary alcohol (e.g. 1-butanol) by hydrogenation of the carbon - oxygen double bond. The reaction is exothermic, but extremely slow in the absence of a catalyst. Carboxylic acids are exceedingly difficult to reduce chemically. Lithium aluminum hydride is one of the few reducing agents capable of reducing a carboxylic acid to a primary alcohol. $LiAlH_4$, however, reacts violently with moisture and would pose a considerable safety threat if used on an industrial scale. Carboxylic acids and alcohols react to form esters in the presence of an acid catalyst, e.g. sulfuric acid which is used as electrolyte in this work, until equilibrium is reached. [5] Chemical reduction doesn't cause a current response, since no explicit electron transfer occur.

Pt is known as an excellent catalyst for breaking C-H bonds in oxidation of methanol and formic acid [13], giving a range of possible reduction reaction product molecules containing more than one carbon atom.

Most carboxylic acids can be reduced to a mixture of carboxylate anion, aldehyde, alcohol or hydrocarbon in a one, two, four or six electron reduction. The complexity of the kinetics vary depending on the acid being studied. [14] It was assumed that butanol is oxidized to butanal and/or butanoic acid, i.e. the reverse of the reduction reactions given in Table 1. Similarly, butanal is expected to oxidize to butanoic acid. While oxidation of butanoic acid would have to involve either the attachment of a new hydroxyl group or the breaking of a C-C bond.

2.2 Calculated standard potentials

The standard reduction potentials of relevant redox reactions were calculated from thermodynamic data [15]. Calculation details are included in Appendix A. The standard reduction potentials were calculated for the direct reduction of formic acid, acetic acid, propionic acid and butanoic acid to their respective alcohols, namely methanol, ethanol, 1-propanol and 1-butanol. It was also calculated for the reduction of butanoic acid to butanal, and butanal to 1-butanol. Table 1 summarize the calculated standard potentials of the respective reactions. The direct reduction of the carboxylic acids to their respective alcohols involve four electrons. While the indirect reduction, via the aldehyde, consist of two steps which involve two electrons each. The calculated standard reduction potentials were used as an estimate of the reduction potentials, although an additional overpotential must be applied for a reaction to happen. It was considered to work with the simplest acids, but since the standard reduction potentials are quite similar butanoic

acid was used. The most positive potential was calculated for the reduction of butanal to 1-butanol. But it's thermodynamically easier to reduce butanoic acid directly to butanol, than to butanal. This may have implications for the reduction mechanism of butanoic acid. A possible mechanism for the reduction of carboxylic acids is proposed in Subsection 5.2.1. The standard reduction potentials are close to the H_2-evolution region. This can render it difficult to decide whether any reduction of organic compounds happened electrochemically at the electrode surface or chemically in the bulk with H_2 as the reducing agent.

Table 1: Standard reduction potentials calculated from thermodynamic data retrieved from ref. [15].

Theoretical cathodic half-reaction	E^o [V vs. SHE]
$HCOOH + 4H^+ + 4e^- \rightarrow CH_3OH + H_2O$	0.110
$CH_3COOH + 4H^+ + 4e^- \rightarrow CH_3CH_2OH + H_2O$	0.034
$CH_3CH_2COOH + 4H^+ + 4e^- \rightarrow CH_3(CH_2)_2OH + H_2O$	0.077
$CH_3(CH_2)_2COOH + 4H^+ + 4e^- \rightarrow CH_3(CH_2)_3OH + H_2O$	0.082
$CH_3(CH_2)_2COOH + 2H^+ + 2e^- \rightarrow CH_3(CH_2)_2CHO + H_2O$	-0.260
$CH_3(CH_2)_2CHO + 2H^+ + 2e^- \rightarrow CH_3(CH_2)_3OH$	0.424
$2H^+ + 2e^- \rightarrow H_2(g)$	0

2.3 Hydrogen evolution reaction (HER) and relevant electrode materials for reduction of carboxylic acids

It is evident from the standard reduction potentials presented in Section 2.2 that H_2-evolution will be a competing reaction because of the low potentials one must go to in order to reduce the organic compounds. Thus an electrocatalyst with a high overpotential against H_2-evolution is needed and preferably high selectivity towards the reduction of carboxylic acids. Adsorption of atomic hydrogen is an intermediate step in the H_2-evolution mechanism. It can be seen from the volcano plot in Figure 1 that metals with intermediate metal - hydrogen bond strength, such as Pt, are the best electrocatalysts for H_2-evolution, i.e. have the highest exchange current densities. If the bond strength is too high will hydrogen be strongly adsorbed and block the active sites towards other processes. Hence, an electrocatalyst that weakly adsorb hydrogen is preferred. Pb and other heavy metals adsorb hydrogen poorly, but were not used in this project due to HSE-concerns. Ag and Cu are examples of safer alternatives. Cu have also shown promising results for the electrochemical reduction of CO_2 [16].

Selectivity is an other important factor which depend greatly on the electrocatalyst, and should be explored in future work. Furthermore, platinum is known to be a good catalyst for dehydrogenation (see methanol oxidation literature [17]), and known to be a stable material in all environments and conditions intended to be used in this work. To limit the scope of the current work only platinum is used as electrode material. Copper was initially investigated in the project work in the fall, but low and nonuniform performance made interpretation difficult. Further work with copper is recommended as it is shown to be a good catalyst for CO_2 reduction [18, 16].

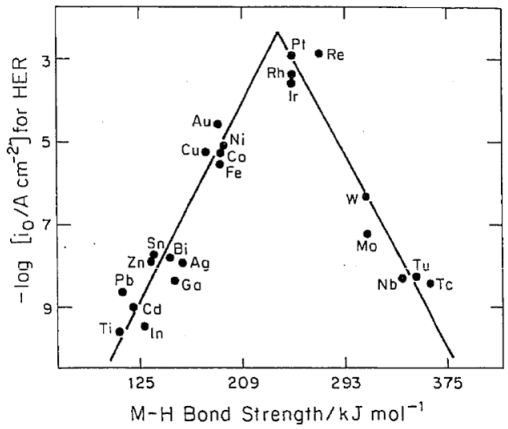

Figure 1: Volcano plot of electrocatalytic activity for the H_2-evolution reaction. [19]

2.4 Linear sweep and cyclic voltammetry (LSV and CV)

A potentiostat is used to apply the desired electrode potential to the working electrode, and for cyclic voltammetry this potential is varied linearly between a negative and a positive reversal or turn-round potential. This is illustrated in Figure 2 where E_t^c represent the negative reversal potential and E_t^a represent the positive one, and ν is the rate of change of potential with time, i.e. sweep rate [20]. Double layer charging will always occur when the potential is changed. The current response is simultaneously registered by the potentiostat. Double layer charging will always occur when the potential is changed, and give a rather small current response. The current response from surface processes, which are dependent of transfer, is proportional to the sweep rate. Mass transport controlled processes, on the other hand, give a current response proportional to the square root of sweep rate. Hence, surface processes will dominate at high sweep rates, and diffusion controlled processes will dominate at low sweep rates. The current is thus determined by the coupling between diffusion and charge transfer at the surface. Various electrochemical reactions give peaks in a voltammogram. The peak potential of fast charge transfer processes is independent of sweep rate, while it's delayed in the sweep direction for slow charge transfer processes. [20]

Rotating the electrode facilitate mass transport to the electrode surface by decreasing the diffusion layer thickness, as discussed in Subsection 2.7. The effect of mass transport can be studied from cyclic voltammograms at different rotation rates.

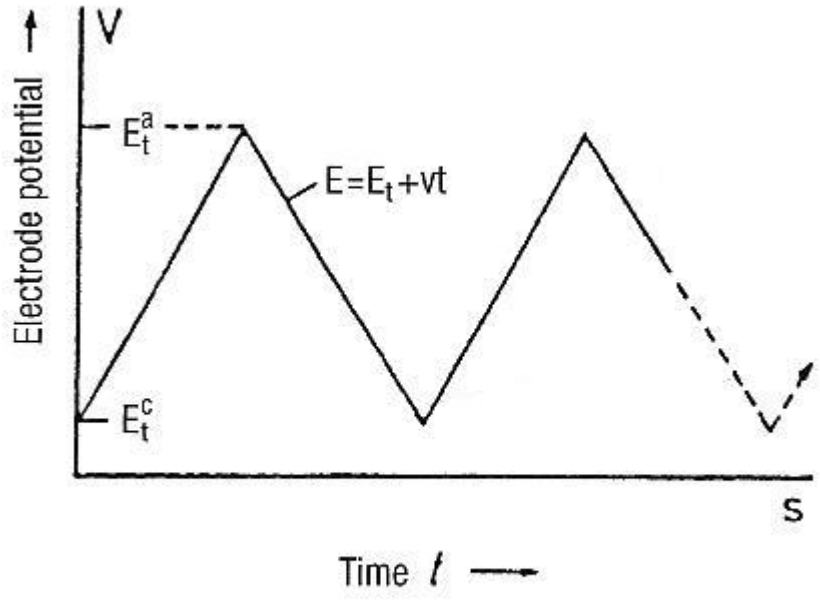

Figure 2: Potential-time behavior at the working electrode following imposition of a triangular waveform typical of cyclic voltammetry. [20]

2.5 Cyclic voltammograms of Pt in base electrolyte

Cyclic voltammogram of Pt in 0.5 M sulfuric acid are given in Figure 3. The lower and upper reversal potentials used were 50 mV and 1.5 V, i.e. the potential window where water is stable for Pt. Outside this window water is split into hydrogen and oxygen gas. At the working electrode H_2 is formed at negative potentials, while O_2 is formed at more positive potential. When sweeping downwards in potential, protons are adsorbed as atomic hydrogen at potentials below 350 mV. After passing the negative turn-round potential, the hydrogen is desorbed again. The adsorption and desorption peaks are fairly symmetrical, hence it happens reversibly. In the potential region from 350-800 mV only charging of the electrolytic double layer occur. Then Pt start to oxidize at approximately 800 mV, forming a passive surface oxide layer. During the return sweep the oxide is reduced at a more negative potential than it was formed, hence the oxide formation is an irreversible reaction. Platinum oxide formation is very complex and have been studied quite thoroughly in the literature, but still without consensus [21]. Adsorption and desorption of hydrogen occur during the negative going sweep and positive going sweep, respectively. The hydrogen underpotential deposition peaks were used to estimate the true active area of the platinum electrode by assuming one hydrogen pr. surface Pt atom, and a surface charge equal to 220 $\mu C\ cm^{-2}$ Pt. See appendix B for how this was done.

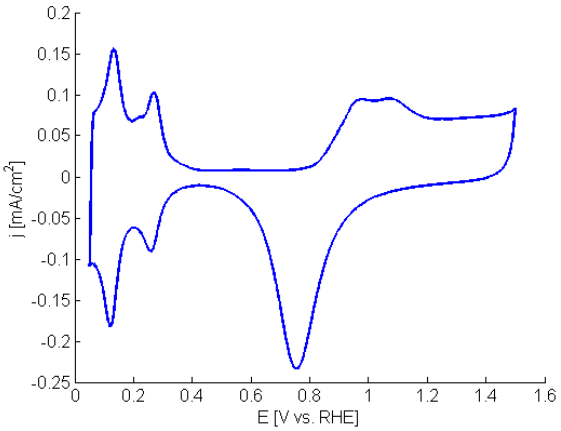

Figure 3: The cyclic voltammogram of Pt at 100 mV/s in 0.5 M H_2SO_4(aq).

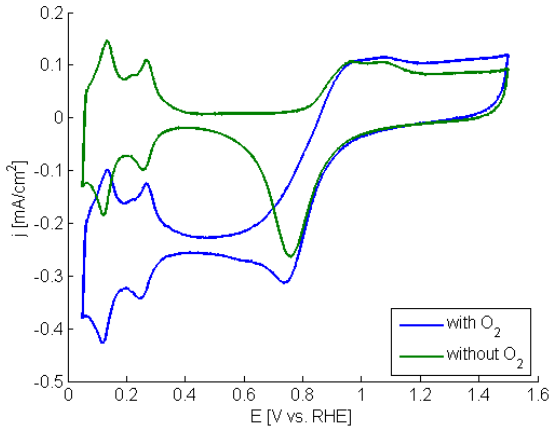

Figure 4: Cyclic voltammogram of Pt in 0.5 M H_2SO_4(aq) at 100 mV/s with and without dissolved oxygen.

2.6 O_2-effect on Pt

The cyclic voltammograms of polycrystalline Pt in blank electrolyte before and after oxygen removal, by purging with Ar(g), are shown in Figure 4. The presence of dissolved oxygen in the electrolyte caused the baseline to shift towards more negative current densities. This is due to the reduction of oxygen:

$$O_2(\text{diss}) + 4\,H^+ + 4\,e^- \rightarrow 2\,H_2O$$

which occurs mainly at potentials in the hydrogen and double layer region. The reduction quickly approaches its limiting current, which depends on the oxygen concentration. Once the oxide is being formed, this process cease to exist, and the voltammetry curves overlap each other independent of oxygen content in the electrolyte.

2.7 Rotating disk electrode (RDE)

Three modes of mass transport are possible, namely migration, diffusion and convection. The primary mass transport mechanism in unstirred solutions is diffusion. One method of effecting convection is with a rotating disk electrode. A sketch of the working end of an RDE is shown in Figure 5. The disk electrode (blue) is embedded in a larger, non-conducting shroud. The entire assembly is rotated. Solution is drawn up along the axis of rotation and past the electrode, so there is laminar flow past the electrode surface. However, the solution at the surface is dragged along by the rotating disk, and there is a thin layer (the Nernst diffusion layer) which is left unstirred. Within this layer, mass transport is by diffusion alone. The effective thickness of this layer depends on the speed of rotation [rpm] of the rotator, the viscosity of the solution, and the diffusion coefficient of the electroactive species. As the rotation speed of the RDE is increased the Nernst diffusion layer becomes thinner. [22] Thus, the mass transport of electroactive species towards the electrode surface can be controlled giving well defined and reproducible mass transport regimes.

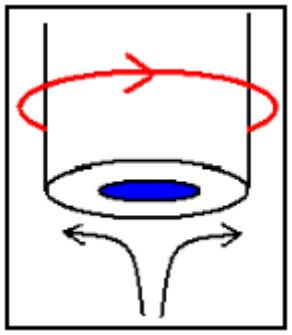

Figure 5: Sketch of the working end of a rotating disk electrode (RDE). [22]

3 Experimental

3.1 Apparatus and Chemicals used

The experimental setup was an AFMSRCE Modulated Speed Rotator setup from Pine. The electrochemical measurements were carried out with a Gamry Instruments Reference 600 potentiostat, utilizing Gamry Instruments Electrochemistry Software Version 5.60. A picture of the setup is given in Figure 6. The experimental data were processed in Echem Analyst, and plotted in Matlab. A one-compartment glass cell was used. A polycrystalline Pt rotating disk electrode from Pine instruments (5 mm in diameter) was used as working electrode (WE). The counter electrode (CE) was a Pt sheet electrode. The reference electrode used was a reversible hydrogen electrode (RHE). Argon gas (Yara, 5.0) was purged through the electrolyte to avoid any influence of oxygen. The base electrolyte was a 0.5 M solution of H_2SO_4 in ion distilled water. The experiments described herein were conducted for two different concentrations, 0.01 and 1.0 M, of each organic specie and in the base electrolyte for comparison reasons. Relevant information about the chemicals used in this work are presented in Table 2.

The IR spectrometer used was an IFS 66v from Bruker, with a mid-IR globar source and a Deuterated Triglycine Sulfate (DTGS) detector with a KBr window [23], that utilizes OPUS software version 6.5. The accessories used were a VeeMAX II ATR Variable Angle, Single Reflection ATR and a VeeMAX Flat Plate 45 degree ZnSe crystal from Pike Technologies.

Table 2: The chemicals used in this work.

Chemical	Formula	Purity	Company name	Hazard
Methanol	CH_3OH	99.8%	Acros Organics	Highly flammable, Toxic
Ethanol	CH_3CH_2OH	$\geq$ 99.9%	Merck	Highly flammable
1-Propanol	$CH_3(CH_2)_2OH$	$\geq$ 99.9%	VWR	Highly flammable, Irritant
1-Butanol	$CH_3(CH_2)_3OH$	$\geq$ 99.5%	Merck	Harmful
Formic acid	H_3COOH	$\geq$ 99%	Acros Organics	Corrosive
Acetic acid	CH_3COOH	100%	VWR	Corrosive
Propionic acid	CH_3CH_2COOH	$\geq$ 99%	Merck	Corrosive
Butyric acid	$CH_3(CH_2)_2COOH$	$\geq$ 99%	Merck	Corrosive
Sulfuric acid	H_2SO_4	96% Suprapur	Merck	Corrosive
Carbon monoxide	CO		Linde	Toxic, Inflammable

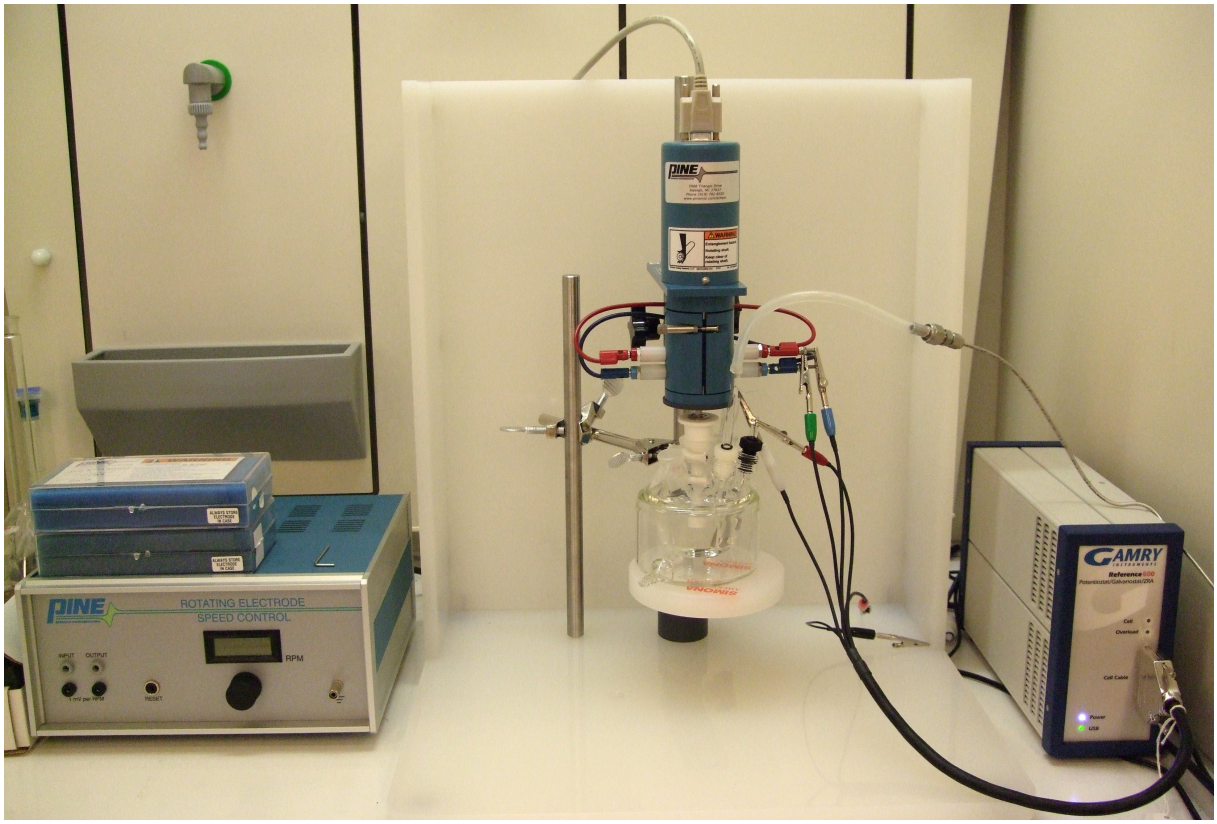

Figure 6: Experimental setup used for the electrochemical measurements. From the left; the rotation speed control unit, the glass cell with all electrodes inserted and the Ar(g) supply connected, and the potentiostat.

The cell and various glass equipment were cleaned in a hot peroxide bath, consisting of 1/4 hydrogen peroxide, 3/4 distilled water, and a small amount of concentrated sulfuric acid, then rinsed thoroughly in ion distilled water.

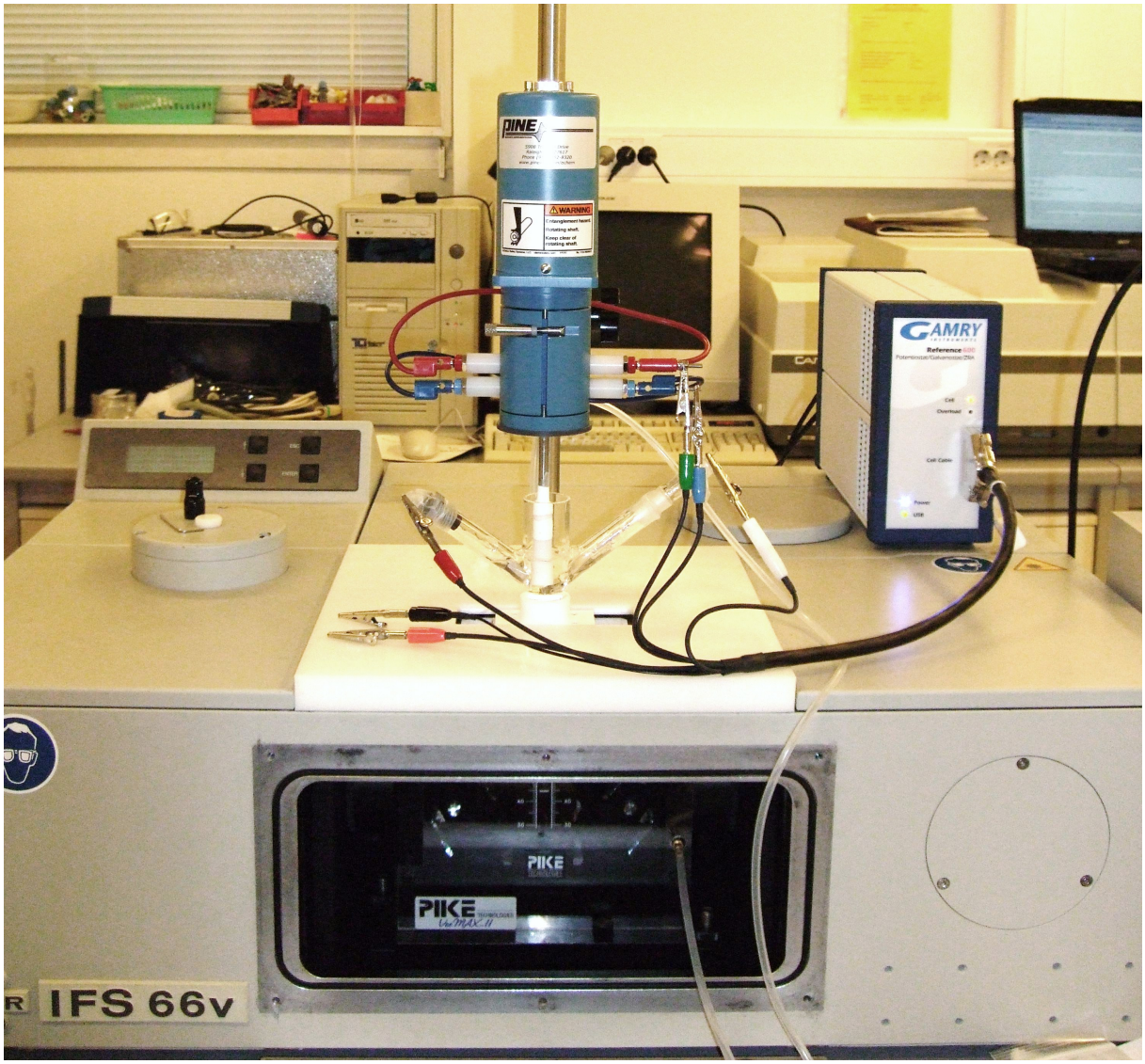

Figure 7: The complete experimental setup used during the FTIRS measurements.

3.2 Experimental program for electrochemical measurements

In order to have a well defined and reproducible surface, the working electrode was cycled at 100 mV/s over an extended period of time (activation) in the base electrolyte before any experiments were conducted. The base electrolyte used in this work was 0.5 M sulfuric acid. Additonal cycling was done after addition of an organic compound. Some voltammograms were then recorded at 100 mV/s, and these voltammograms were used to calculate the active surface area for hydrogen adsorption, as shown in Appendix B. Thereafter the experiments were performed. All experiments were conducted at room temperature. The cyclic voltammograms shown are stationary unless otherwise is stated. Potentials in this work are all quoted against a reversible hydrogen electrode (RHE) in the same solution, for which H_2-evolution will always take place thermodynamically at 0 V [20]. All reported current densities are calculated from the true active surface area, determined by integrating the hydrogen adsorption peaks at 100 mV/s and assuming a charge density for a smooth platinum surface of 220 $\mu C\ cm^{-2}$. See Appendix B for how this was done.

The open circuit potential (OCP) was measured before, during and after addition of each organic compound to the base electrolyte. About 1600 rpm rotation was used for mixing the electrolyte. The initial and final potential was 0.4 V vs. RHE for the cyclic voltammetry experiments, and reduction processes were promoted by sweeping in the negative direction first. All parameters were varied in a random order to avoid systematic errors.

3.2.1 Oxidation experiments

Cyclic voltammetry measurements at 10 and 100 mV/s for a variable number of the rotation rates in Table 3 were conducted in 1 M ethanol and for both concentrations of propanol, butanol and the carboxylic acids. The increasing positive turn-round potential (E_{upper}) experiment described in Figure 8 was conducted in 0.01 and 1.0 M of 1-propanol (up to 1.1 V) and all four carboxylic acids. The reported CVs from the increasing positive turn-round potential experiments are not stationary. A linear sweep voltammetry experiment is described in Table 4.

Table 3: Cyclic voltammetry experiments. The negative and positive turn-round potentials were 0.05 V and 1.5 V vs. RHE, respectively.

Effect of:	Sweep rate [mV/s]	Speed of rotation [rpm]
Sweep rate	10, 20, 50, 100, 200, 500, 1000	-
Rotation	10,100	0, 100, 900, 2500

Table 4: Linear sweep voltammetry experiments. The positive potential limit was 1.5 V vs. RHE.

Effect of:	Hold-time [s]	Hold-potential [mV vs. RHE]	Sweep rate [mV/s]	Rotation [rpm]
Rotation	300	50	10	0, 2500

3.2.2 Reduction experiments

The cyclic and linear sweep voltammetry experiments are summarized in Table 5 and 6. Gas bubbles were removed from the electrode surface by high speed rotation at about 0.2-0.3 V vs. RHE in the positive going sweep. Cyclic voltammetry measurements at 10 mV/s for different negative turn-round potentials or rotation rates in Table 5 were only conducted in propionic and butyric acid. The electrode potential was held at 0 V over night ($\geq$ 14 hours) in 1 M of propionic acid or butyric acid. Then cyclic voltammetry (100 mV/s) was conducted after a few minutes at OCP.

Table 5: Cyclic voltammetry experiments. The positive turn-round potential was 1.5 V vs. RHE.

Effect of:	E_{lower} [mV]	Sweep rate [mV/s]	Rotation [rpm]
E_{lower}	-150, -100, -50, 0, 50	50	Gas bubble removal
E_{lower} & Rotation	-50, 0, 50	10	2500
Rotation	0	10	0, 100, 900, 2500

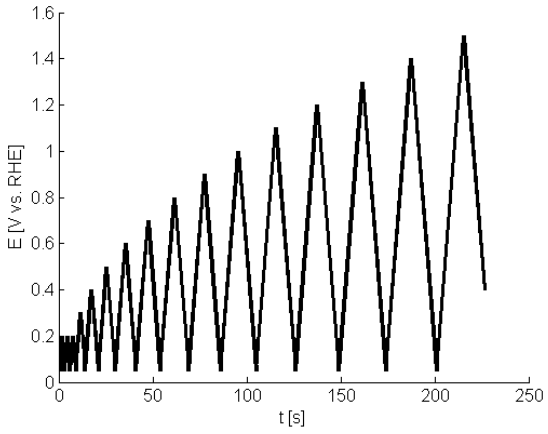

Figure 8: Programmed potential-time behaviour of the potentiostat during variable E_{upper} measurements.

Table 6: Linear sweep voltammetry experiments. The negative and positive potential limits were -100 mV and 1.5 V vs. RHE, respectively.

Effect of:	Hold-time [s]	Sweep rate [mV/s]	Rotation [rpm]
Hold-time	0, 5, 10, 30, 60, 90, 120, 180, 240, 300	10	Gas bubble removal

3.3 Design and development of setup for external reflectance FTIRS

One objective for the cell design was to be able to use as much as possible of the equipment already available at the laboratory. The final setup includes the rotator, Pt RDE, RHE and CE described in Section 3.1, which were used for the electrochemical part of this work. The rotator acted as WE holder which allowed for moving the WE up and down as well as rotation. The cell itself was made from glass while the cell holder, which was screwed to a commercial crystal (ZnSe) plate during IR experiments, was made from Teflon. The holder and cell were threaded for easy assemblage and disassembling for cleaning. The counter and reference electrode were placed as low as possible to minimize ohmic drop from the electrolyte. A new top lid for the sample compartment of the spectrometer, with a hole for the cell, that also served as a stand for the rotator was fabricated from a polyoxymethylene (POM) plate and a steel bar. The complete setup with the VeeMAX II mirror unit constitute an external reflection configuration with a ZnSe ATR crystal.

Teflon tape was applied to the glass threads before assemblage to prevent leakage. An O-ring in combination with a (home-made) Parafilm gasket was used as seal between the cell holder and crystal plate. At first the Parafilm gasket center hole diameter was less than the RDE sheath diameter, to give reproducible electrolyte thickness for when the WE was pressed down on to the crystal. But this was later changed so the electrolyte thickness became reduced.

Rotation of the RDE will stir oxygen into the electrolyte due to the cell being open to the atmosphere, thus rotation should be limited to the removal of gas bubbles evolved at the electrode surface. A plastic pipette should be used for purging of the entire electrolyte volume, due to the high placing of the gas inlet, while ensuring no scratching of the crystal surface. However, this gas inlet position render possible vigorous Ar purging without disturbing the electrolyte close to the WE.

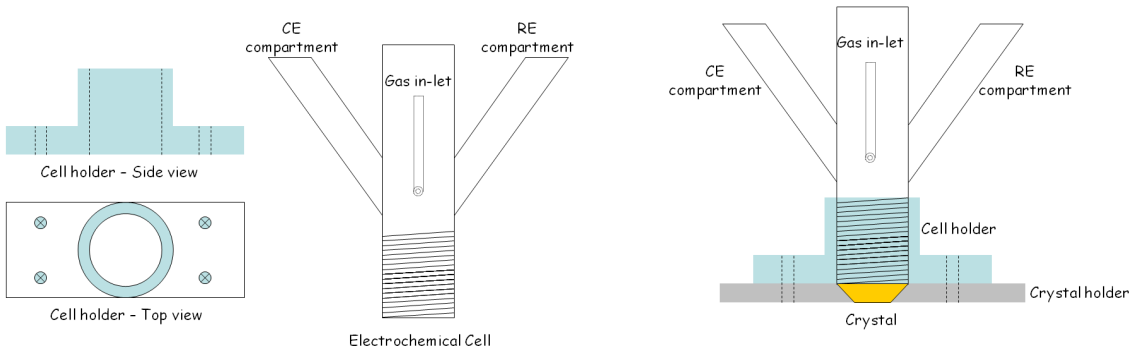

Figure 9: Schematics of cell design illustrating (a) individual pieces designed, (b) assembled with the commercial crystal, and (c) WE positioned for IR scanning.

3.4 Experimental program for IR related measurements

Testing of the custom IR cell's electrochemical properties, in base electrolyte, and possible leakage with regard to ohmic drop causing possible shift in peak potentials with a cell bottom made from Teflon. The setup used for this testing and the commercial ZnSe crystal used as the cell bottom, i.e. window, during the IR experiments is shown in Figure 10. Cyclic voltammograms with the WE well separated from the Teflon bottom (i.e., under non-contact conditions) and when the WE was in close contact with the Teflon bottom (i.e., under contact conditions) at both 10 mV/s and 100 mV/s were obtained.

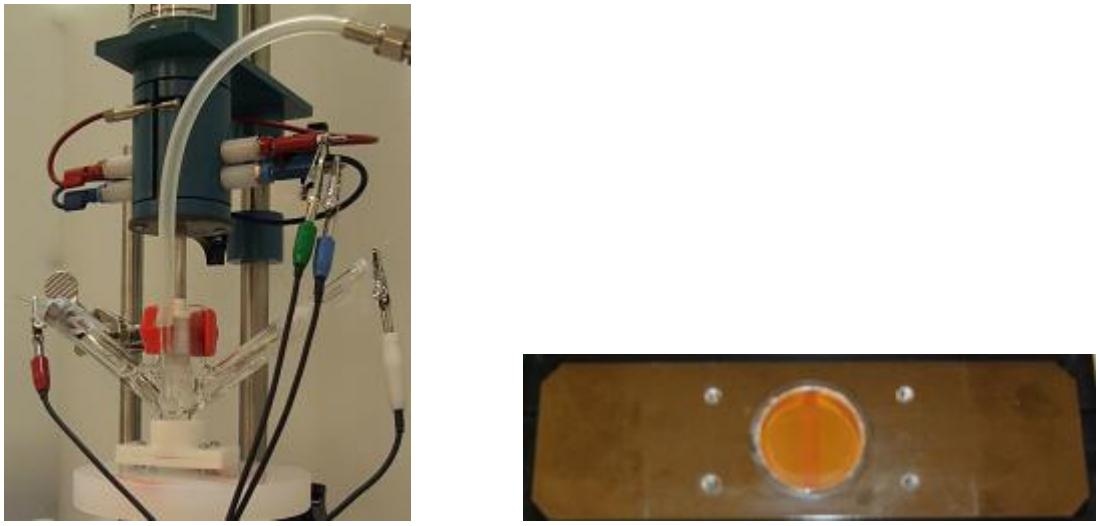

(a) (b)

Figure 10: (a) Custom-made glass cell for IR experiments assembled with electrodes and connected to a Teflon bottom for testing of electrochemical properties and possible leakage. (b) The commercial ZnSe crystal used as the cell bottom, i.e. window, during the IR experiments.

The procedures used during the experiments of which the results are given in Subsection 4.3 were developed through trial and error and are not optimal. The mirror unit was adjusted according to the manual, except the set incident angle was left constant at about 45 degrees, which is the optimum angle with regard to signal intensity. Both chronoamperometric and linear sweep type experiments were conducted in 1 M methanol, but are not included in the results. The procedures used during the experiments of which the results are given in Subsection 4.3 were developed through trial and error, in base electrolyte with and without methanol, and are not optimal. The platinum WE was cleaned by cycling the potential (50 cycles) between 0.05 and 1.5 V. Then gaseous CO was purged through the electrolyte for >20 minutes before and during measurements. The imposed potential-time behaviour of the platinum WE during the reported chronoamperometric and linear sweep voltammetry experiments is illustrated in Figure 11. Both background and sample spectra were obtained while the Pt WE RDE was in close contact with the ZnSe crystal. Background spectra were obtained at an electrode potential of 50 mV and

full CO coverage. During the potential step procedure in Figure 11a spectra were obtained under steady state conditions by averaging 200 scans. The adsorption potential (50 mV) was applied for 3 minutes and spectra were recorded after about 100 s at each potential. During the linear sweep the repeated measurements option within OPUS [24] was utilized. Spectra were obtained continuously by averaging 10 scans pr. spectrum. Scanning was initiated while at 50 mV. The resolution was 4 cm^{-1} and the scan speed 10 kHz in both cases.

The absorbance spectra were calculated automatically by OPUS, and all reported spectra have been subjected to a mathematical algorithm within OPUS which corrected for bands from water vapour and aqueous solution [24].

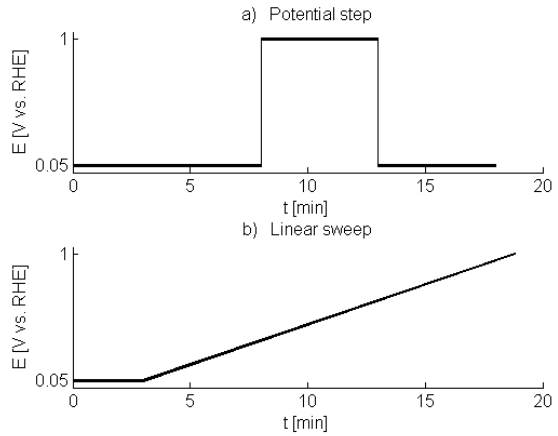

Figure 11: Electrochemical procedure during IR-scanning, (a) potential step or (b) slow linear sweep (1 mV/s) initiated after 3 minutes at the adsorption potential.

4 Results

4.1 Oxidation processes

4.1.1 Alcohols

Figure 12 show cyclic voltammograms (10 mV/s) of a Pt rotating disk electrode in sulfuric acid with presence of methanol, ethanol, 1-propanol and 1-butanol at both 0.01 and 1 M in the potential window where water is stable. The base voltammogram without any organic compound present is included in the same figure for comparison reasons. The measured current density at potentials positive to 0.8 V can be looked upon as the sum of two overlying oxidation processes, platinum oxide formation (see base voltammogram Figure 12e) and oxidation of organic species. Similarly, between 1.0 V and 0.6 V in the negative going sweep, the measured current density is the sum of reduction of surface oxide and oxidation of organics. The response is quite similar in shape for the four alcohols with two oxidation peaks in the positive scan direction and one peak in the negative scan direction, after sufficient platinum oxide has been reduced. In the positive going sweep, with 0.01 M of the different alcohols, the anodic current response commences at potentials around 0.6 V, and diminishes when the formation of platinum oxide begins at 0.9 V. After a minimum around 1.1 V a second peak occur. Both methanol and ethanol at 1 M display a shoulder at 0.7 V prior to the first peak. In 0.01 M a small cathodic peak from the reduction of formed platinum oxide can be seen in the reverse sweep at 0.8 V immediately before oxidation commence again. This reduction peak is not observed for 1 M of any of the alcohols at this sweep rate. The relative sizes of the anodic peak current densities vary for the different alcohols, sweep rate and with concentration. The first oxidation peak is reduced to a shoulder in 1 M of butanol. The peaks are shifted towards higher potentials in higher concentration, while the peak current densities are significantly larger in 1 M compared with 0.01 M. The response in the hydrogen underpotential deposition (H_{UPD}) region diminishes for high alcohol concentration.

The effect of increasing sweep rate is presented in Figures 13-14 for 0.01 M and 1 M of alcohols. Faster sweep rates in 0.01 M of methanol (Figure 13a) give less blockage, hence more distinct hydrogen adsorption and desorption peaks. The anodic peaks in the positive going sweep are indistinguishable for the highest sweep rates in 0.01 M, making the voltammograms resemble the one for the base electrolyte. The effect of increasing sweep rate is more clear in Figure 14 for 1 M of alcohols. It can be seen from this figure that the oxidation peaks in the positive going and negative going scan increase and become delayed with increasing sweep rate. Corresponding figures presenting this effect with the current density normalized to 100 mV/s with respect to charge is included in Appendix C.1.1.

4.1.2 Carboxylic Acids

Cyclic voltammograms at 10 mV/s without rotation for a Pt disk electrode in a sulfuric acid (0.5 M) electrolyte with presence of either 0.01 and 1 M of formic acid, acetic acid, propionic acid and butyric acid, are given in Figure 15 for potentials between the hydrogen and oxygen evolution onset potentials. Formic acid differs from the other acids, which contain more than one carbon. Two oxidation peaks in the positive scan direction and one larger peak in the negative scan direction, after sufficient platinum oxide has been reduced, are observed for both concentrations of formic acid. A positive current is observed in the high potential region during the reverse sweep, until about 1.3 V. The current density is nearly 20 times higher in 1 M formic acid relative to 0.01 M, however, the peaks are delayed for the higher concentration in a similar way as for the alcohols. Acetic, propionic and butyric acid show low reactivity at the potentials swept over and any oxidation commences close to 1.0 V in the positive going sweep, when significant oxide has formed. An oxidation peak is observed for these acids at around 1.3 V at this sweep rate, far into the oxide region. Little response is observed in the reverse sweep for these acids. However, the oxide reduction peak is slightly smaller compared to in the base electrolyte. Acetic acid is the least reactive of the acids and display only insignificant changes in current response with concentration. Propionic and butyric acid are oxidized more easily than acetic acid. They also display an increase in oxidation current density along with a small decrease in the oxide reduction peak for the higher concentration. An additional cathodic current response in the H_{UPD} region was observed for 1 M of propionic and butyric acid.

The higher the sweep rate in 0.01 M of the respective carboxylic acids, see Figure 16, the more the acid voltammograms resemble the base electrolyte.

From Figure 17, it can be observed that both the forward and the backward anodic peaks for 1 M formic acid increase up to a point with increasing sweep rate. The current density increase all the way round for 1 M of the other acids. Corresponding figures presenting this effect with the current density normalized to 100 mV/s with respect to charge is included in Appendix C.1.1.

Voltammograms of 0.01 and 1 M propionic and butyric acid, respectively, at 100 mV/s with the positive turn-round potential increased by increments of 0.1 V are shown in Figure 18. The imposed potential-time function giving rise to the plotted voltammograms is also included. The voltammograms for 0.01 M are virtually equal to the base electrolyte. In 1 M the oxidation of propionic and butyric acid commence at roughly 1 V and the oxide reduction peak is significantly smaller compared to the base electrolyte. A small increase in the cathodic current response in the H_{UPD} region with increasing upper potential limit is observed for the 1 M solutions.

4.1.3 Open circuit potentials

Figure 19 show the change in open circuit potential upon adding the various carbonaceous species into the base electrolyte. The alcohols studied all display an abrupt fall in the open circuit potential upon addition. Formic acid display similar behaviour as the alcohols, while the acids with more than one carbon atom only give an insignificant change in the open circuit potential upon adding them to the base electrolyte.

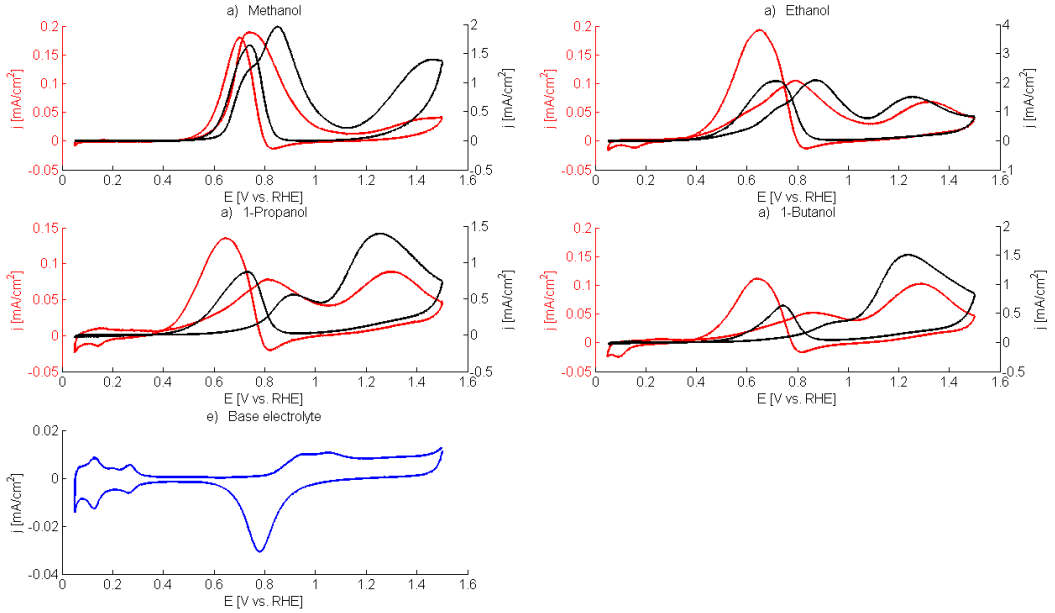

Figure 12: Cyclic voltammograms at 10 mV/s in 0.01 M (red) and 1 M (black) of (a) methanol, (b) ethanol, (c) 1-propanol, (d) 1-butanol and (e) the base electrolyte (0.5 M sulfuric acid).

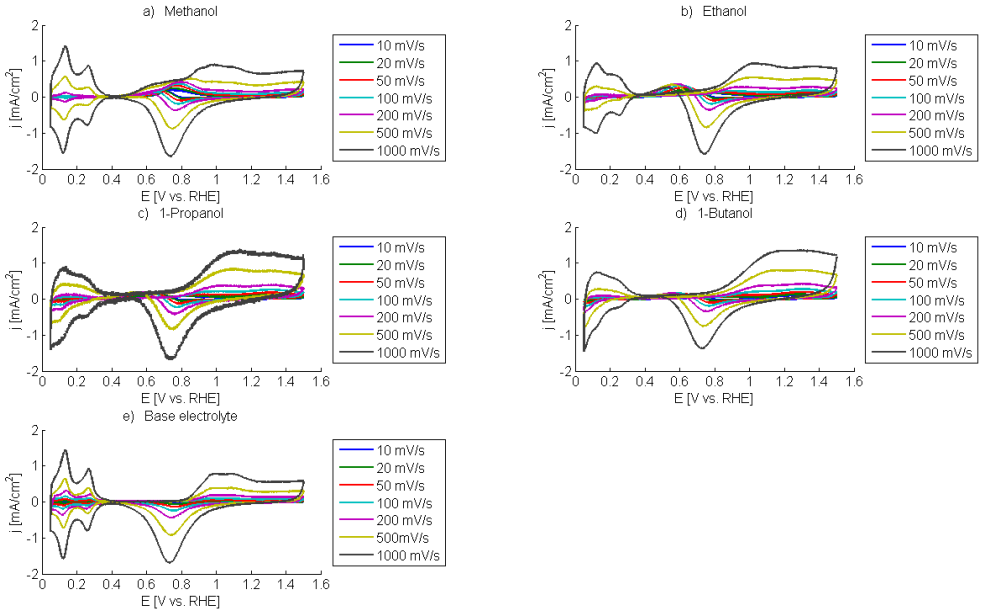

Figure 13: Effect of sweep rate in the presence of 0.01 M of (a) methanol, (b) ethanol, (c) 1-propanol, (d) 1-butanol and (e) the base electrolyte, not normalized with respect to sweep rate.

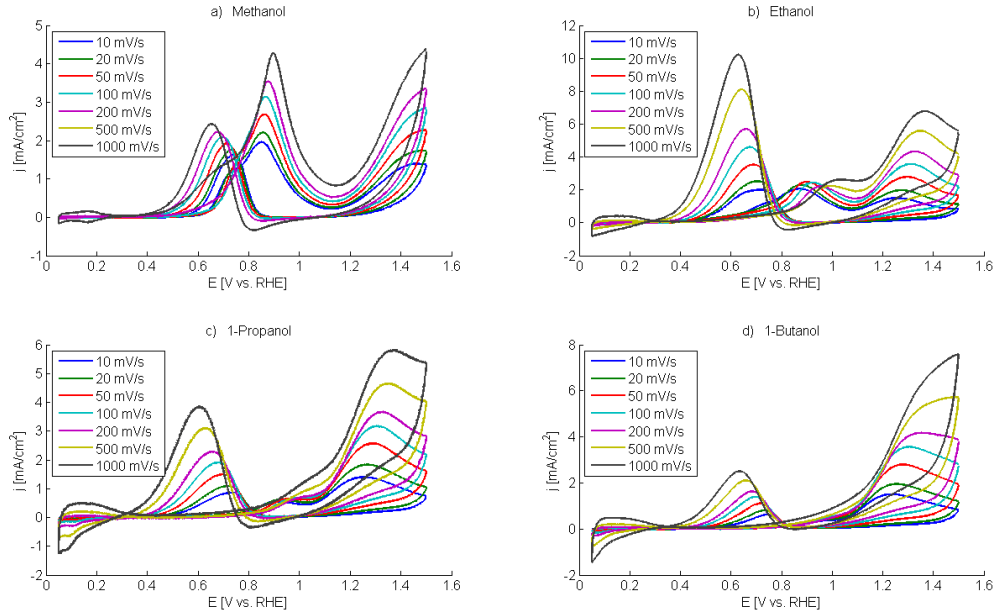

Figure 14: Effect of sweep rate in the presence of 1 M of (a) methanol, (b) ethanol, (c) 1-propanol, (d) 1-butanol, not normalized with respect to sweep rate.

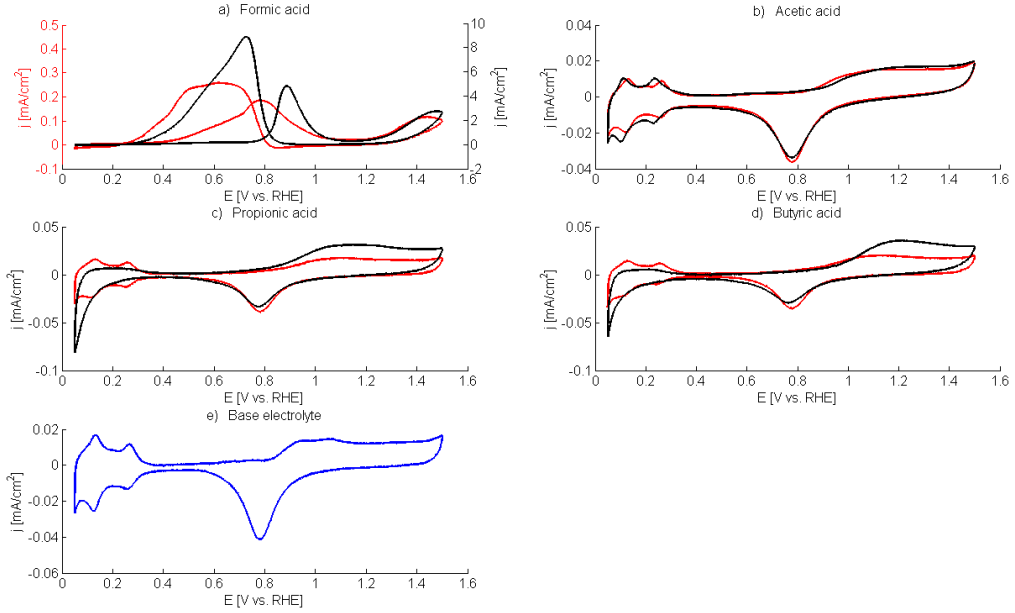

Figure 15: Cyclic voltammograms at 10 mV/s in 0.01 M and 1 M of (a) formic acid, (b) acetic acid, (c) propionic acid (d) butyric acid and (e) the base electrolyte (0.5 M sulfuric acid).

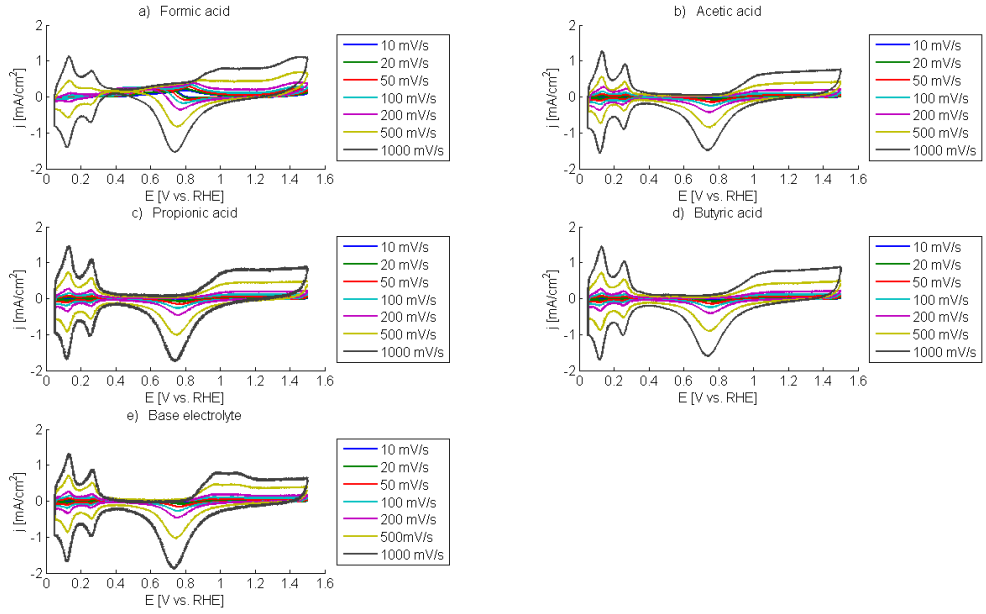

Figure 16: Effect of sweep rate in the presence of 0.01 M of (a) formic acid, (b) acetic acid, (c) propionic acid and (d) butyric acid and (e) the base electrolyte, not normalized with respect to sweep rate.

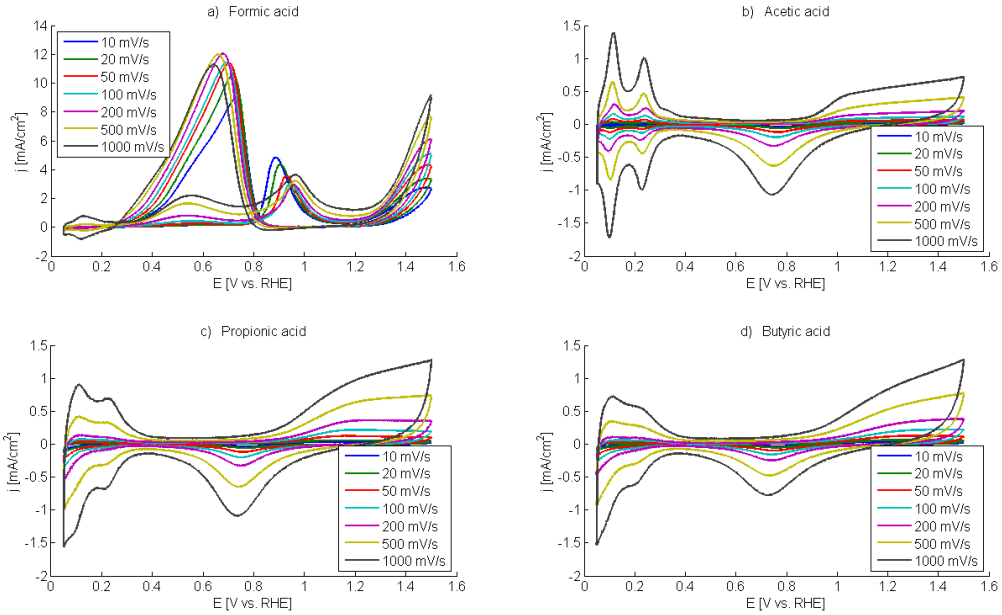

Figure 17: Effect of sweep rate in the presence of 1 M of (a) formic acid, (b) acetic acid, (c) propionic acid and (d) butyric acid, not normalized with respect to sweep rate.

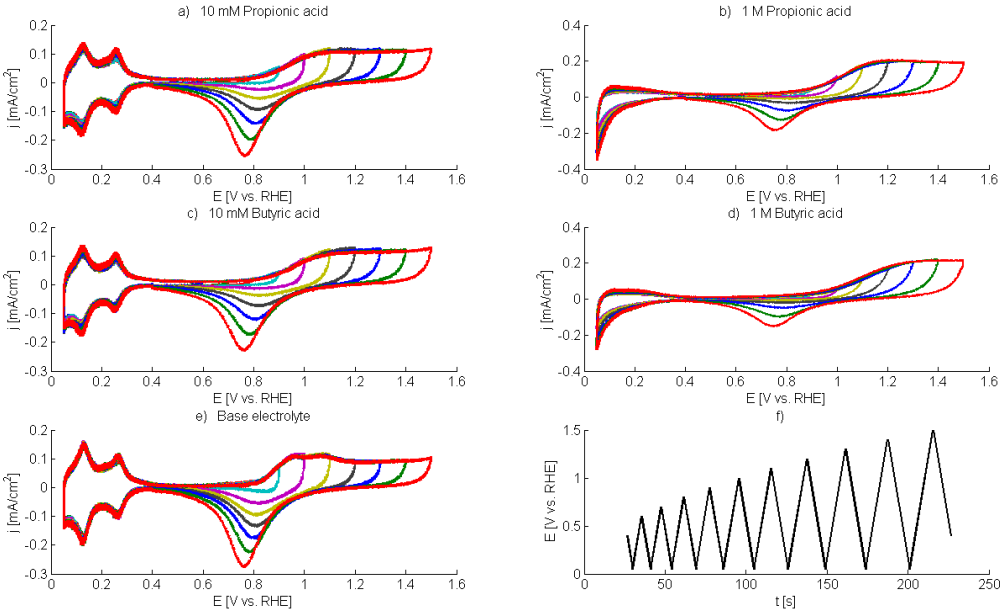

Figure 18: Voltammograms at 100 mV/s with the positive turn-round potential increased by increments of 0.1 V for each cycle, from 0.6 V to 1.5 V, in (a) 0.01 M and (b) 1 M of propionic acid, (c) 0.01 M and (d) 1 M of butyric acid, and in (e) the base electrolyte, (f) the imposed triangular wave giving these results.

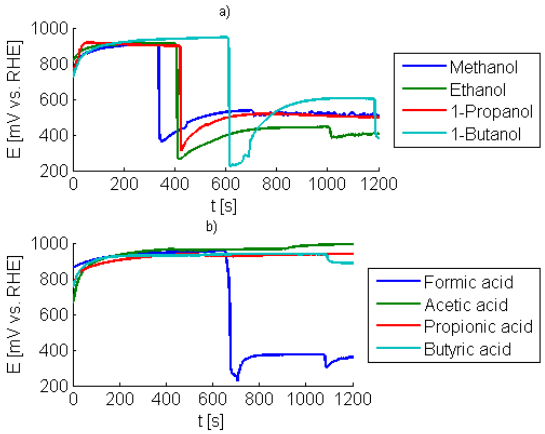

Figure 19: Change in open circuit potential upon addition of (a) alcohols and (b) carboxylic acids to the base electrolyte.

4.2 Investigation of processes in the H_{UPD} and H_2 evolution reaction region (HER)

CVs with more negative turn-round potentials are displayed in Figures 20-23 for 0.01 M and 1 M of alcohols and 0.01 M and 1 M of carboxylic acids, respectively. Compared to similar experiment in base electrolyte only, no additional cathodic current response was observed for 0.01 or 1 M of any of the alcohols or carboxylic acids studied in this work. On the contrary a passivation towards HER of the electrode was observed for 1 M of the alcohols (Figure 21) and carboxylic acids (Figure 23). The passivation is most pronounced for methanol and formic acid. The hydrogen oxidation peak current (E > 0) is larger for the higher concentration of propanol, butanol and acetic, propionic and butyric acid despite the reduced cathodic current relative to the base electrolyte. Although it's not clear from these figures, the current response at potentials positive to 0.4 V, after removal of gas bubbles, was not affected by the lowered negative turn-round potential.

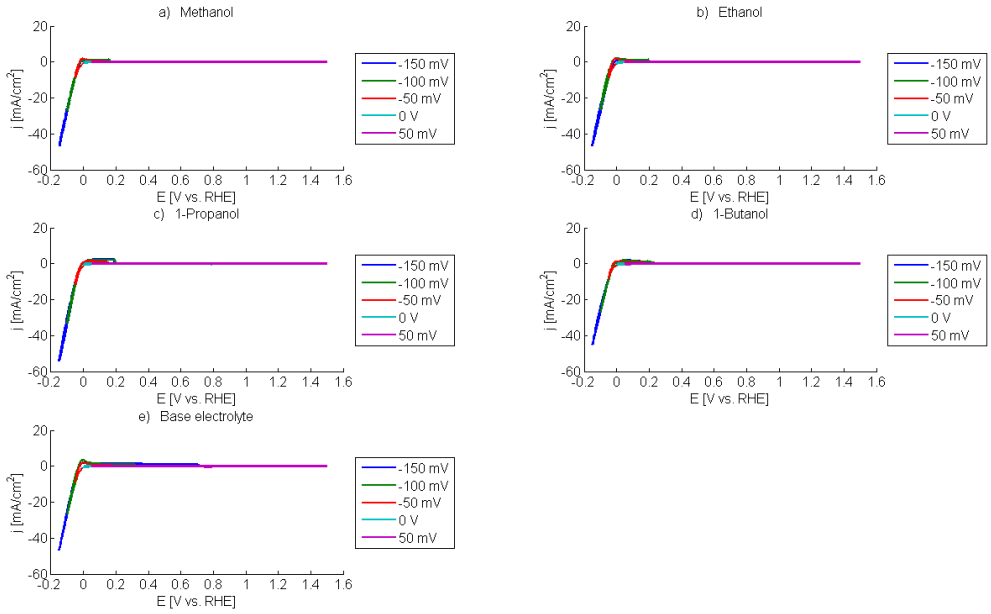

Figure 20: Cyclic voltammograms at 50 mV/s with various negative turn-round potentials in 0.01 M of (a) methanol, (b) ethanol, (c) 1-propanol, (d) 1-butanol and (e) the base electrolyte.

Linear sweep voltammograms initiated after holding the potential at -100 mV for variable lengths of time are presented in Figures 24-27 for 0.01 M and 1 M of alcohols and 0.01 M and 1 M of carboxylic acids, respectively. No trend or correlation with hold-time at -100 mV was observed for the oxidation of the carbonaceous species. Extensive hydrogen evolution occurred at this negative potential.

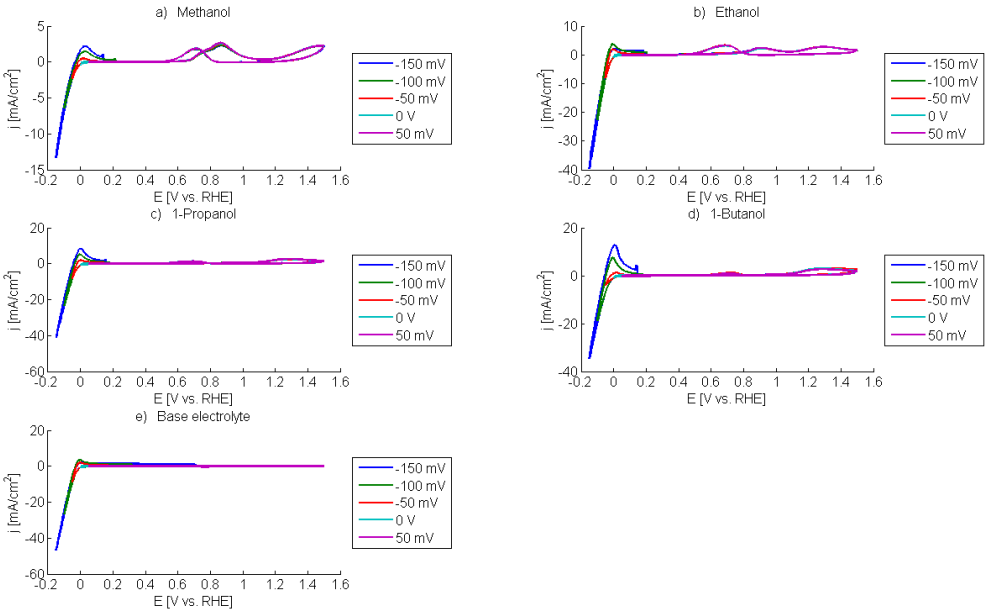

Figure 21: Cyclic voltammograms at 50 mV/s with various negative turn-round potentials in 1 M of (a) methanol, (b) ethanol, (c) 1-propanol, (d) 1-butanol and (e) the base electrolyte.

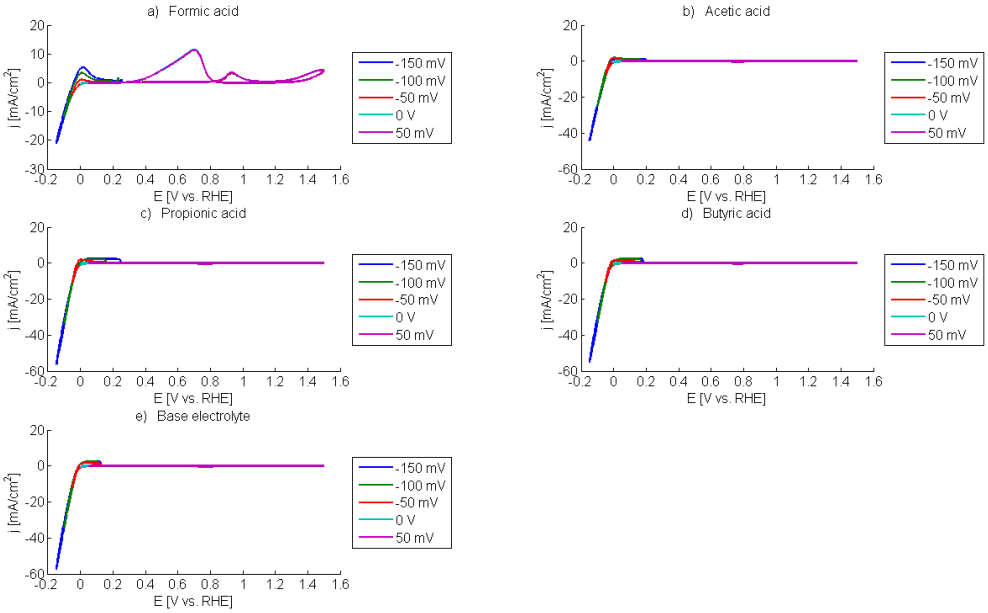

Figure 22: Cyclic voltammograms at 50 mV/s with various negative turn-round potentials in 0.01 M of (a) formic acid, (b) acetic acid, (c) propionic acid and (d) butyric acid and (e) the base electrolyte.

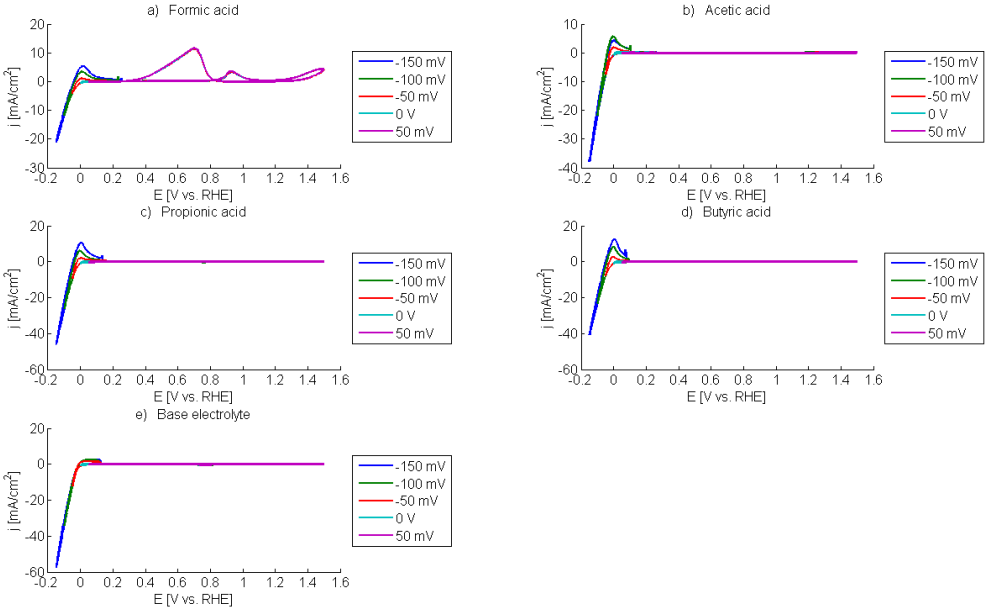

Figure 23: Cyclic voltammograms at 50 mV/s with various negative turn-round potentials in 1 M of (a) formic acid, (b) acetic acid, (c) propionic acid and (d) butyric acid and (e) the base electrolyte.

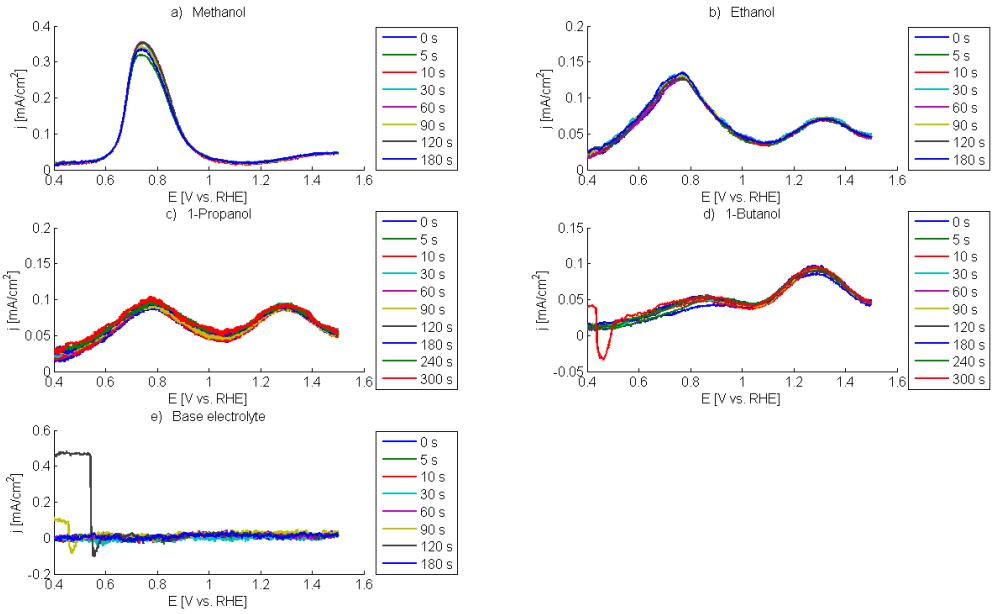

Figure 24: Linear sweep voltammograms at 10 mV/s following various holding times at -100 mV in 0.01 M of (a) methanol, (b) ethanol, (c) 1-propanol and (d) 1-butanol and (e) the base electrolyte. Potentials below 0.4 V are omitted for clarity.

Figure 28 show the first two cycles of the CVs in 1 M propionic and butyric acid after sitting at 0 V and 2500 rpm over night (14 hours), and a few minutes at OCP. Nothing interesting was observed for propionic acid. In the case of butyric acid, two additional anodic peaks in the forward sweep and one additional cathodic peak in the reverse sweep was observed. The first anodic peak, positioned at 585 mV, is the largest (1.0 $mAcm^{-2}$). A second anodic peak (0.43 $mAcm^{-2}$) occur at 960 mV. The reverse sweep elapse as usual until a second peak occur at 569 mV (-0.23 $mAcm^{-2}$) where nearly all the oxide is reduced.

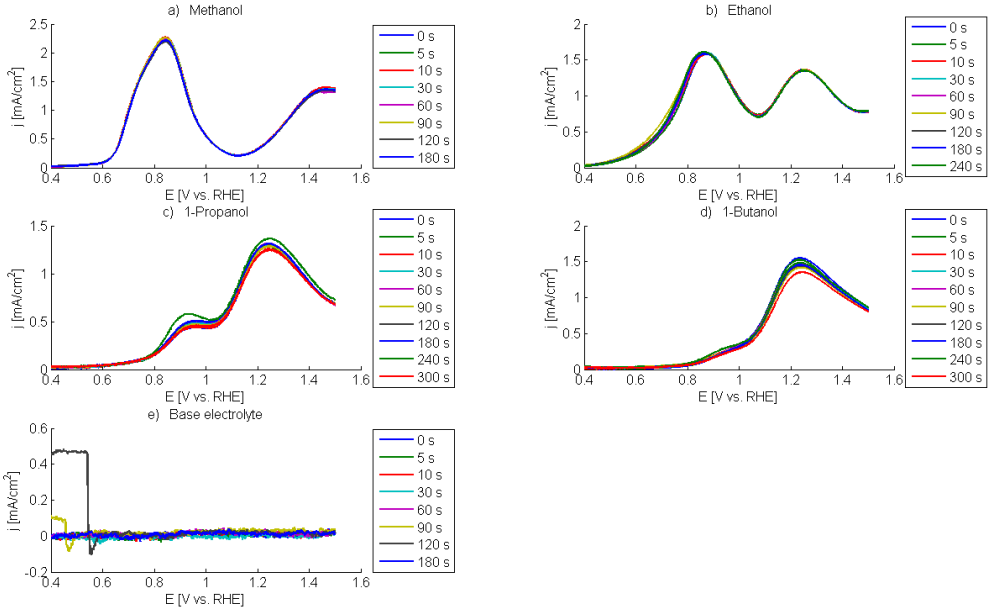

Figure 25: Linear sweep voltammograms at 10 mV/s following various holding times at -100 mV in 1 M of (a) methanol, (b) ethanol, (c) 1-propanol and (d) 1-butanol and (e) the base electrolyte. Potentials below 0.4 V are omitted for clarity.

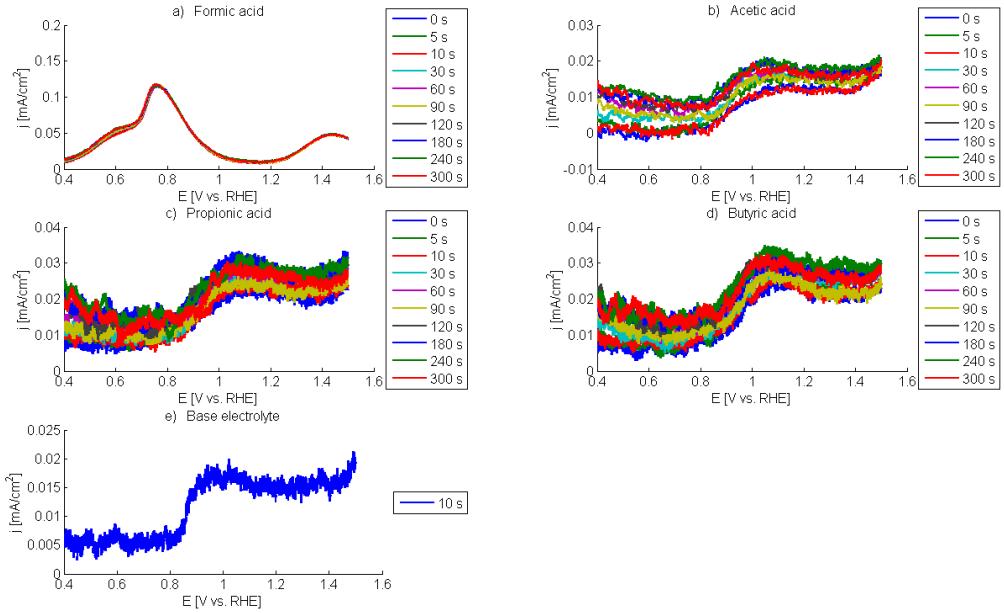

Figure 26: Linear sweep voltammograms at 10 mV/s following various holding times at -100 mV in 0.01 M of (a) formic acid, (b) acetic acid, (c) propionic acid and (d) butyric acid and (e) the base electrolyte. Potentials below 0.4 V are omitted for clarity.

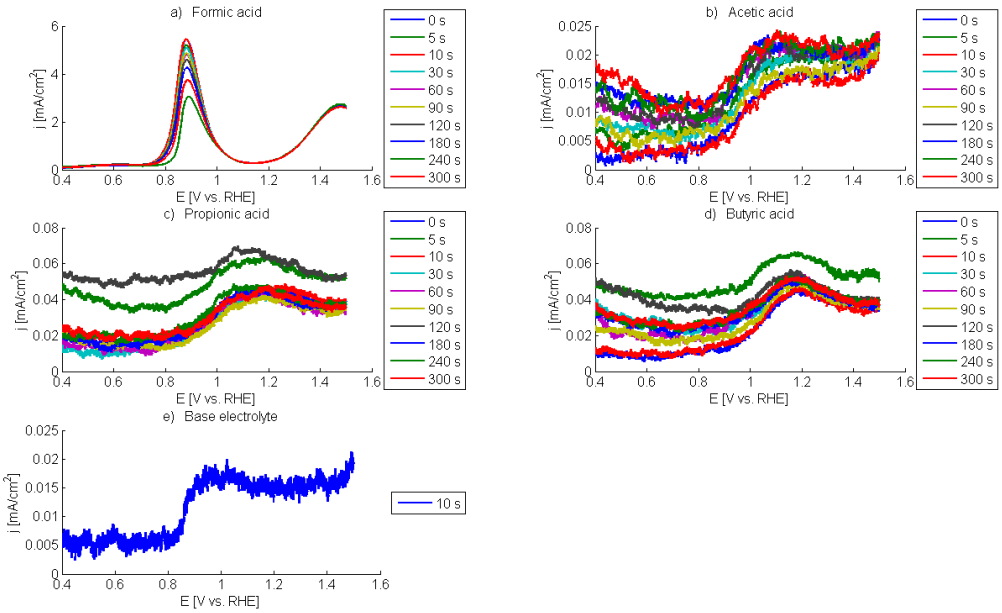

Figure 27: Linear sweep voltammograms at 10 mV/s following various holding times at -100 mV in 1 M of (a) formic acid, (b) acetic acid, (c) propionic acid and (d) butyric acid and (e) the base electrolyte. Potentials below 0.4 V are omitted for clarity.

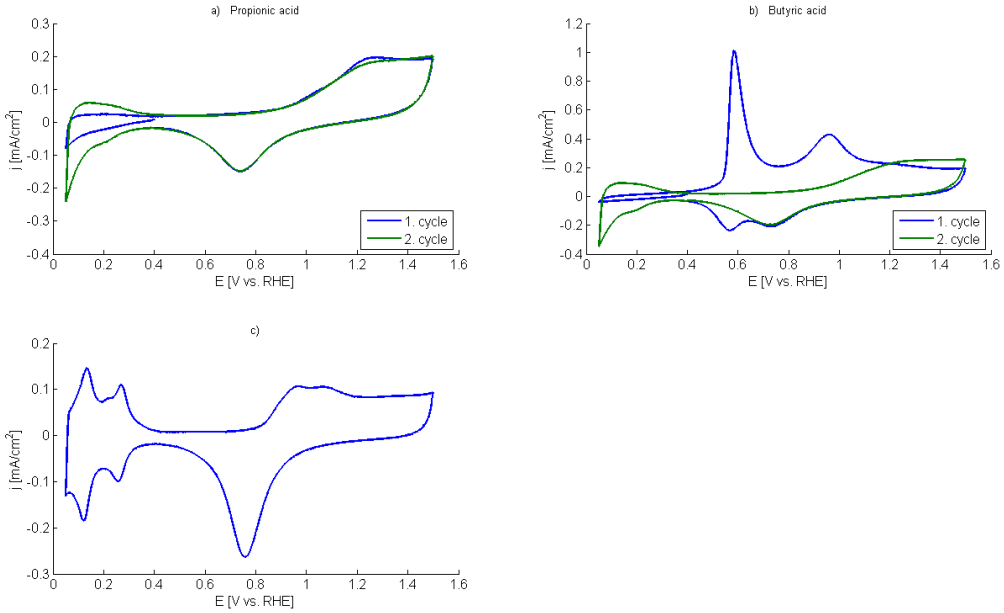

Figure 28: Cyclic voltammograms at 100 mV/s after holding at 0 V and 2500 rpm overnight in 1 M of (a) propionic acid, (b) butyric acid and (c) a stationary cyclic voltammogram in the base electrolyte.

4.3 Preliminary IR results

Testing of the custom IR cell with regard to ohmic drop causing shift in peaks was conducted with a cell bottom made from Teflon. Cyclic voltammograms with the WE well separated from the Teflon bottom (i.e., under non-contact conditions) and when the WE was in close contact with the Teflon bottom (i.e., under contact conditions) at both 10 mV/s and 100 mV/s are shown in Figure 29. The CVs look good with only minor differences between the contact and non-contact conditions. The Teflon tape need to be replaced often, to ensure no leakage.

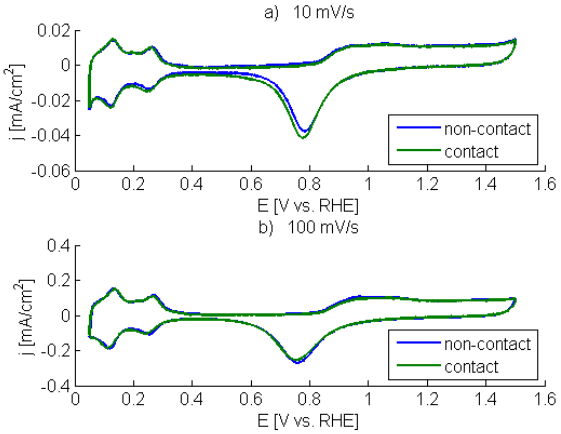

Figure 29: Cyclic voltammograms using the custom designed IR cell while the WE and Teflon bottom were well separated (i.e., under non-contact conditions) and when the WE was in close contact with the Teflon bottom (i.e., under contact conditions) at (a) 10 mV/s and (b) 100 mV/s.

No CO related peaks were observed in IR spectra of 1 M methanol present in the electrolyte (not shown). Linear sweep voltammograms following 3 minutes at 50 mV in CO saturated electrolyte with and without a Parafilm gasket are presented in Figure 30. The CO stripping peak with Parafilm between the WE sheath and the crystal was followed by mass transport limited CO-bulk oxidation current density. Removing the Parafilm allowed for close(r) contact between the WE and the crystal, and no bulk oxidation was observed due to having a CO concentration in the thin electrolyte layer lower than bulk concentration.

Even without the Parafilm no CO related peaks were observed in the corresponding IR spectra at 45 ° set incident angle, only variable peaks from dissolved CO_2 (2300-2400 cm^{-1} [25]) and in the wavenumber region related to adsorbed (bi-)sulfate (1100-1300 cm^{-1} [7]), see Figure 31.

The signal amplitude without electrolyte was maximized for 53 degrees. Promising peaks in the wavenumber region related to adsorbed CO [25, 7], shown in Figure 32, was observed at this incident angle. However, the observed intensity was very weak. The signal

amplitude had deteriorated with time from a value of ca. 3250 during initial test scans to less than 2400 when the spectra given in Figure 32 were obtained.

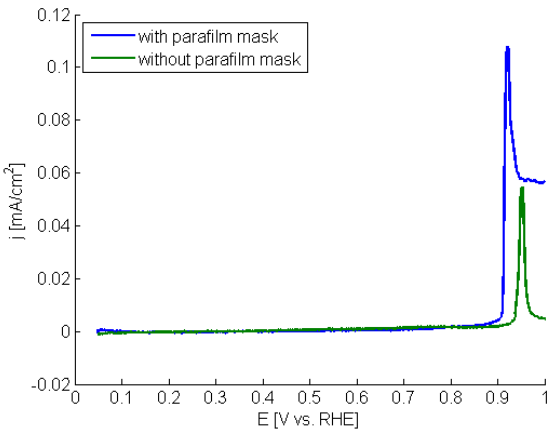

Figure 30: Slow linear sweep voltammograms (1 mV/s) after holding at 50 mV for 3 minutes in CO saturated electrolyte, with and without a Parafilm mask.

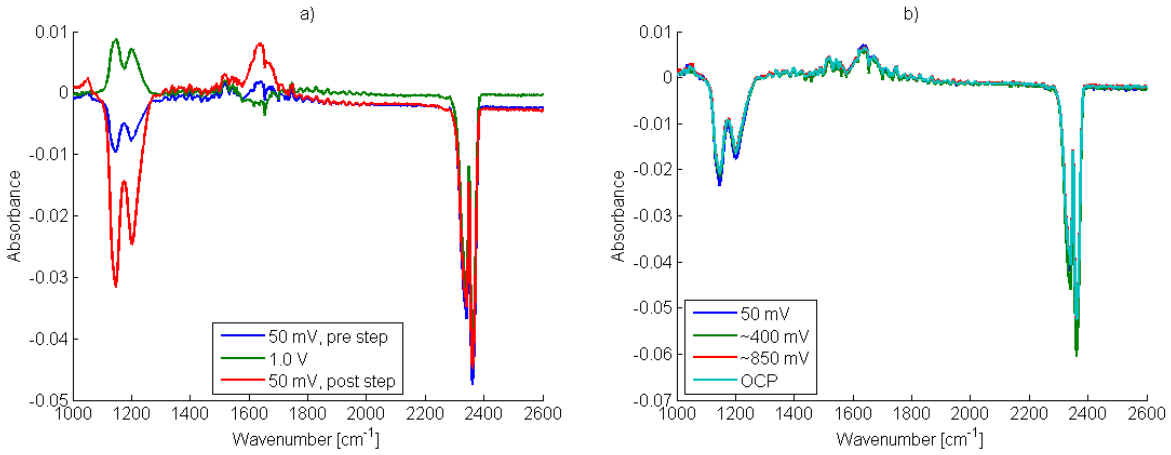

Figure 31: Infrared spectra with 45 ° set incident angle in CO-saturated electrolyte at various potentials during (a) the chronoamperometric experiment and (b) the linear sweep experiment illustrated in Figure 11.

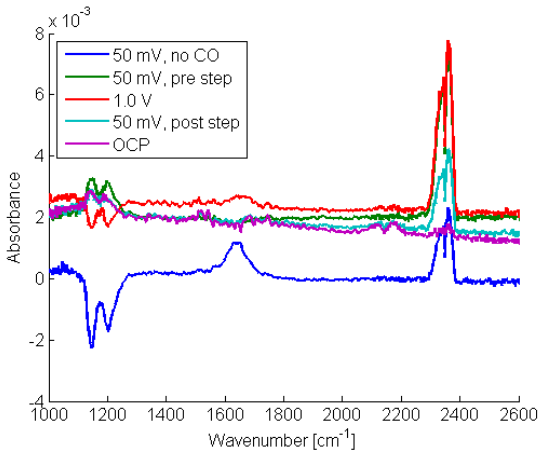

Figure 32: Infrared spectra with 53 ° set incident angle in 0.5 M sulfuric acid (blue) and in CO-saturated electrolyte at various potentials during the chronoamperometric experiment illustrated in Figure 11a.

5 Discussion

5.1 Oxidation processes

5.1.1 Alcohols

Figure 12 summarizes the differences and similarities between the four alcohols studied, and also display the effect of concentration for each of them. Higher concentration of alcohols rendered higher oxidation current densities, due to more alcohol being available for oxidation, and a shift of peaks towards more positive potentials in the forward scan and towards more negative potentials in the reverse scan, respectively. The latter is connected with the mechanism of oxidation, i.e. the competition for active sites between the adsorption processes. The following discussion will concern the mechanism for oxidation of methanol since it has been the topic of numerous studies, see references [26, 27, 28, 29, 30, 31] and references therein.

$$\mathrm{Pt} + \mathrm{CH_3OH} \rightarrow \mathrm{CO(ads)} + 4\mathrm{H^+} + 4\mathrm{e^-} \quad (1)$$

$$\mathrm{Pt} + \mathrm{H_2O} \rightarrow \mathrm{OH(ads)} + \mathrm{H^+} + \mathrm{e^-} \quad (2)$$

$$\mathrm{CO(ads)} + \mathrm{OH(ads)} \rightarrow \mathrm{CO_2} + \mathrm{H^+} + \mathrm{e^-(rds)} \quad (3)$$

Equation 1 and 2 are competing electrochemical adsorption reactions, both dependent on potential as driving force. Formation of adsorbed CO (reaction 1) dominates at low potentials (below about 0.55 V) resulting in a surface completely covered with CO, and thus formation of an oxygen containing surface species such as OH(ads) (reaction 2) is the limiting step for the complete oxidation to CO_2. Once oxide is readily formed at more positive potentials step 3 becomes rate determining. The current density increases with increased number of OH(ads) until an optimum surface condition is reached. When the formation of oxygen take over at even more positive potentials, the current density decreases again and a peak is formed. This main oxidation peak is not dependent on mass transport, but is the result of an optimum surface state, and therefore do not scale with the square root of sweep rate (not shown here). Kinetic calculations for CO oxidation at a Pt electrode from dissolved CO in electrolyte results in a current when for $\theta_{\mathrm{CO}} = \theta_{\mathrm{OH}} = 0.5$ [17]. The current peak potential, hence where the optimum surface state is achieved, is shifted to more positive potentials by concentration. The methanol adsorption is made more competitive as the concentration is increased and the optimum surface condition is thus shifted to more positive potentials. The second anodic peak in methanol is due to the transition from a less active to a more active surface oxide, and not competition as for the first peak since Reaction 2 is fast in this potential range. Platinum oxide formation is very complex and have been studied quite thoroughly in the literature, but still without consensus [21]. The role of oxidation states of the platinum surface in electrocatalytic oxidation of small primary alcohols, however, have been studied by Li et al. [32]. Oxide

must be reduced in the reverse sweep in order to reactivate the surface, hence oxidation commence after sufficient oxide is reduced . This is most easily seen for low concentrations and/or higher sweep rates, where the beginning of the oxide reduction peak can be seen. The anodic peak form when the optimum surface condition is restored once more, before Reaction 1 again dominate and full CO coverage is re-established.

Brateng [33] have studied electrooxidation of both methanol and ethanol by use of potential step/sweeps and quartz crystal microbalance (EQCM). And a comprehensive review of the oxidation of small organic molecules as studied by in situ infrared spectroscopy is given by Sun [34]. Methanol is different from the longer alcohols in that it has only a single carbon, yielding CO as the principal adsorbed intermediate, and small amounts of formyl. The mechanism for ethanol, on the other hand, is more complex because ethanol contains two carbon atoms so the C-C bond has to be broken to oxidize ethanol completely to CO_2. Breaking the C-C bond proved difficult and the presence of other adsorbates than CO was observed. Ethanol is therefore normally oxidized to acetaldehyde or acetic acid, directly or via the aldehyde. The mechanism for propanol and butanol, with three and four carbon atoms, respectively, are expected to ethanol, although potentially even more complex due to the increasing number of possible electron transfers. Similar features of the forward scan regarding the surface oxide formation were observed for methanol, ethanol, 1-propanol and 1-butanol by Li et al. [32] as well as in this work (Figures 12,13,14), indicating that the oxidation mechanism for propanol and butanol is similar to the one for ethanol. Thus yielding the corresponding aldehyde and carboxylic acid, respectively, as the principal oxidation products. Oxidation of alcohol to aldehyde happen in one step involving 2 electrons, and two steps involving 2 electrons each give the carboxylic acid. The decrease in peak current density with increasing number of carbon atoms, can perhaps be explained by steric hindrance preventing all the active sites from being accessed.

5.1.2 Carboxylic Acids

Figure 15 summarizes the differences and similarities between the four carboxylic acids studied, and also display the effect of concentration for each of them. Ionization of the carboxylic acids is ignored in this work since they're studied in the presence of the much stronger sulfuric acid (pH$<$1). Formic acid stand out with its single carbon, analogous to methanol. The oxidation mechanism of formic acid involve a direct and an indirect path, as presented in Figure 33 and Equations 4 and 5. The subsequent oxidation of CO for the indirect path is analogous to Reaction 3 discussed above.

$$\mathrm{HCOOH} \rightarrow \mathrm{CO(ads)} + \mathrm{H_2O} \quad (4)$$

$$\mathrm{HCOOH} \rightarrow \mathrm{CO_2} + 2\mathrm{H^+} + 2\mathrm{e^-} \quad (5)$$

The C-C bond appear not to have been broken in the carboxylic acids either. Oxidation

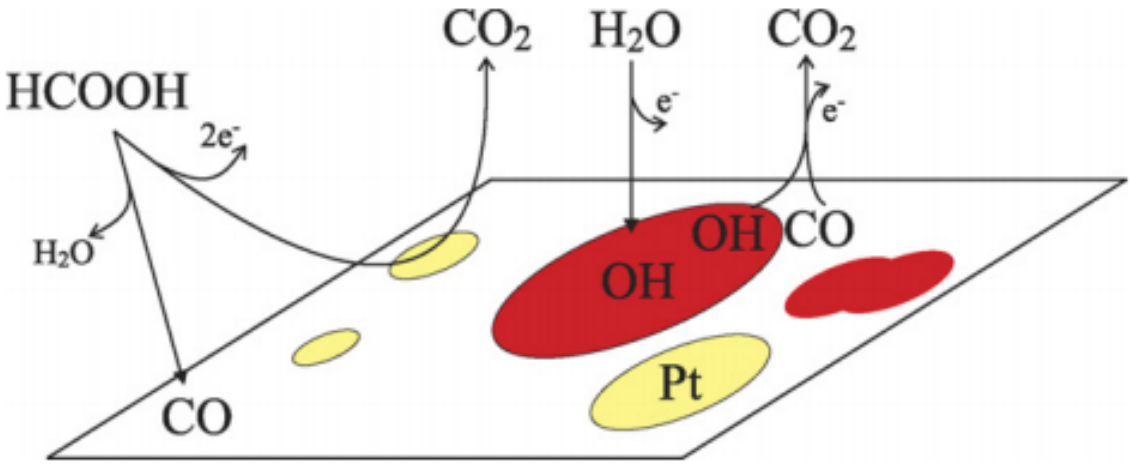

Figure 33: Schematic of the mechanism. Formic acid reacts in the direct pathway to CO2 via free Pt sites (yellow regions) or dissociates to adsorbed CO (uncoloured region of the surface). Adsorbed CO and OH (red regions) react at island edges to give CO2, completing the indirect pathway. [35]

of the carboxylic acids with two or more carbons commenced well into the oxide region, when/where the surface was (partially) covered with oxide. The observed oxidation current response increased with the carbon chain length, from negligible in acetic acid at both concentrations to noticeable in 1 M of propionic and butyric acid. This correspond well with the acidity, which decrease due to increased stabilization of the carboxyl group from the carbon chain of increasing length through electron displacement towards the carbonyl carbon. The oxide reduction peak was slightly smaller compared to in the base electrolyte, indicating that some oxide was consumed during oxidation of carboxylic acid. The acid molecules are expected to coordinate themselves with the oxide covered surface, as well as each other [5], through hydrogen bonding. Then the acid molecule may somehow bend in a way that allow for donation of an oxygen containing species to the carbon furthest away from the carboxyl group forming a hydroxy acid. Steric hindrance may also play a role in this, as this step will become less feasible close to the bulky carboxyl group. Note that this is a working hypothesis, which need to be tested in future work.

The magnitude of the change in open circuit potential (OCP) correlate well with the ease of which the different carbonaceous species are oxidized. The potential at the moment when the carbonaceous species were added to the base electrolyte was about 0.9 V (i.e. OCP in base electrolyte). Upon closer inspection of the voltammograms of alcohols and acids, Figure 12 and 15, it become apparent that no oxidation of acetic, propionic nor butyric acid occur at this potential. This probably mean no formation of strongly bonded adsorbates occurred which would affect the double layer and thus the open circuit potential.

5.1.3 Effect of sweep rate and positive turn-round potential, with special focus on the H_{UPD} region

A clear change in the hydrogen underpotential deposition (H_{UPD}) region with concentration was observed for acetic, propionic and butyric acid. In 1 M of propionic and butyric acid (Figure 15) an interesting additional cathodic current response was observed. What caused it is unknown. The standard reduction potentials for ROOH $\rightarrow$ ROH suggest it could be the desired reduction reaction. It could also be some kind of adsorption process. The OCP of these acids, however, suggest no adsorption interaction between the platinum surface and the acid, but this cathodic current response was observed at significantly lower potential and after cycling of the potential. This reduction or adsorption process is discussed further in Subsection 5.2.

The increase in current density with increasing sweep rate is due to a proportionality between current density and sweep rate. While the changing appearances of the peaks are due to less time for the respective reactions to occur. Low sweep rate mean more time and better opportunity for the respective reactions to occur, giving rise to more distinct peaks. Only methanol cause full blockage in the H_{UPD} region for both concentrations at the low sweep rates. While at the highest sweep rates there's not enough time to adsorb CO in the reverse sweep and the active sites are left available for hydrogen adsorption. This was also the case for the strongly adsorbed species from the other alcohols. Oxidation of ethanol yield some CO and strongly adsorbed acetate/acetaldehyde [33]. Propanol and butanol are expected to give similar species. The blockage of the H_{UPD} region remain relatively unaltered by sweep rate for the alcohols except methanol, i.e. the process seems to be more or less independent of the amount reacted or produced. A minor change was observed for butanol, possibly due to a chemical adsorption step independent of potential and surface state.

Formic acid differ from the other carboxylic acids studied in this work for the same reason as methanol stand out from the alcohols. Little change was observed for the acids, except formic acid. Hence the process yielding the cathodic current response in the H_{UPD} is independent of sweep rate. It is, however, dependent on rotation and concentration, see Appendix C.1.3), which means it's influenced by mass transport and/or involve a chemical step. The difference in oxide reduction peak current density was apparent for all the sweep rates in acetic, propionic and butyric acid. Normalized voltammograms are shown in Appendix C.1.1.

It is evident from Figure 18 that moving the positive turn-round potential to more positive potentials lead to an increase in the quantity of surface oxide formed and consequently in the subsequent reduction peak. The oxide reduction peak is absent when the positive turn-round potential is negative to 0.9 V, below which little Pt oxide formation occur. Variation of the upper potential limit affected oxidation and reduction processes, as well as the H_{UPD} region, in presence of propionic and butyric acid. The observed decrease in

corresponding charge of the oxide reduction peak, and that this became more pronounced with increasing length of carbon chain, support the above proposed mechanism for carboxylic acid oxidation. This effect points to the oxidation being a surface process under activation control. The change in the H_{UPD} region with upper potential limit is related to the observed effects of sweep rate and rotation (see Appendix C.1.3). The connection between the upper potential limit, i.e. oxide formation, and the change in adsorption of H^+ and evolution of H_2 is not clear. More experiments are necessary to investigate whether this process is something which take place only in the hydrogen region, or in relation to oxide or other processes occurring at more positive potentials.

5.2 Electrode processes in the H_{UPD} and H_2 evolution reaction (HER) region

Cyclic voltammograms with more negative turn-round potentials was presented in Figures 20-23. The respective current densities at the negative turn-round potentials are summarized in Table 7. Little change was observed in the reactivity. Some blockage of active sites was evident in the 1 M solutions, more so for the alcohols than the carboxylic acids. Methanol and formic acid gave the highest degree of blockage in the HER region, as expected due to the easy formation of strongly adsorbed intermediate (CO). This means that instead of an increased cathodic current for the acids in the HER region, a passivation of the electrode occurred. (Rotation had no further effect, see Appendix C.2.)

Little or no effect of the hold-time at -100 mV on the linear sweep response was observed. Extensive hydrogen evolution occurred at this negative potential. Hence, a small current measuring resistance had to be chosen that could be susceptible to pick up noise and be inaccurate, in particular in the low current region. An automatic resistor option is possible, but resulted generally in more noise due to small uncorrected variations in the values. During the project work last fall an electrolyte sample were taken after reduction experiments were carried out in butyric acid, and sent to Statoil Research Center at Rotvoll for gas chromatography analysis. The only organic compounds detected, however, were the ones manually added. This indicated that electrochemical reduction might be difficult.

The long-term experiment in 1 M butyric acid (Figure 28) caused a significant change in the subsequent CV. The unknown adsorbed species were present after several minutes at OCP, which suggests that the OCP was quite low (≤ 0.5 V vs. RHE) in their presence. One possibility is that reduction of butyric acid have produced the unknown species. But the fact that the additional peaks only were observed during the very first sweep, and not the following sweeps, show that sitting at 0 V and 2500 rpm over night only produced surface adsorbed species and not significant amounts of any dissolved products. Reproduction of this experiment in an in-situ FTIR setup could perhaps reveal the identity of the adsorbed

Table 7: Cathodic current densities at the different negative turn-round potentials for the cyclic voltammograms of (a) alcohols and (b) acids displayed in Figures 20-23.

(a)

E_{lower}	Base electrolyte	Methanol [$mAcm^{-2}$]		Ethanol [$mAcm^{-2}$]		1-Propanol [$mAcm^{-2}$]		1-Butanol [$mAcm^{-2}$]	
[mV]	[$mAcm^{-2}$]	0.01 M	1 M	0.01 M	1 M	0.01 M	1 M	0.01 M	1 M
50	-0.05966	-0.01714	-0.01736	-0.06467	-0.08054	-0.09354	-0.09381	-0.1282	-0.09688
0	-0.6742	-0.6453	-0.3405	-0.7294	-0.7840	-0.9363	-0.7999	-0.6375	-0.8377
-50	-8.575	-8.663	-2.321	-8.779	-7.963	-11.43	-7.931	-8.059	-3.879
-100	-26.46	-27.10	-6.424	-26.68	-22.53	-33.11	-22.96	-26.66	-18.86
-150	-46.52	-46.89	-13.27	-46.45	-39.61	-54.26	-40.56	-44.75	-34.54

(b)

E_{lower}	Base electrolyte	Formic acid [$mAcm^{-2}$]		Acetic acid [$mAcm^{-2}$]		Propionic acid [$mAcm^{-2}$]		Butyric acid [$mAcm^{-2}$]	
[mV]	[$mAcm^{-2}$]	0.01 M	1 M	0.01 M	1 M	0.01 M	1 M	0.01 M	1 M
50	-0. 07767	-0.03347	-0.03247	-0.08025	-0.08687	-0.08649	-0.2232	-0.08949	-0.1761
0	-0. 7947	-0.4596	-0.4596	-0.6371	-0.6522	-0.8088	-0.9226	-0.7267	-0.9091
-50	-11. 52	-4.024	-4.024	-7.897	-7.344	-10.47	-9.133	-10.14	-7.596
-100	-33. 76	-11.61	-11.61	-24.49	-21.37	-33.14	-25.91	-32.51	-22.76
-150	-56. 70	-21.47	-21.47	-43.80	-37.62	-55.78	-45.44	-54.62	-40.18

species.

5.2.1 Possible mechanism for reduction of carboxylic acids

The observed additional cathodic current response in the H_{UPD} region might be from the reduction of carboxylic acid. Adsorption of propionic and butyric acid, and hydrogen as shown in Reaction (6) and Reaction (7) occurred in the reduction experiments. The adsorption of carboxylic acid explain the observed passivation of Pt during the reduction experiments. How and if propionic and/or butyric acid was reduced in any of the experiments is uncertain. But it may have happened as described in Reaction (8). Hydrogen evolution (Reaction (9) [1]), which is a competing reaction to the reduction of carboxylic acid, did definitely occur at the Pt electrode surface.

$$\mathrm{ROOH(bulk) + S} \rightarrow \mathrm{ROOH(ads)} \quad (6)$$

$$\mathrm{H^+ + e^- + S} \rightarrow \mathrm{H(ads)} \quad (7)$$

$$\mathrm{2H(ads) + ROOH(ads/bulk)} \rightarrow \mathrm{H_2O + ROH + 3S} \quad (8)$$

$$\mathrm{2H(ads)} \rightarrow \mathrm{H_2(g) + 2S} \quad (9)$$

Significant amounts of hydrogen was produced on Pt. This may have resulted in chemical reduction in the bulk electrolyte, as in Reaction (10).

$$\mathrm{ROOH(bulk) + H_2(g)} \rightarrow \mathrm{ROH + H_2O} \quad (10)$$

The electrochemical reduction of carboxylic acids cannot be ruled out since the standard potential values say the reaction is thermodynamically possible. Slow kinetics, however may render it difficult to achieve. Since Pt is well known as a good catalyst for H_2-evolution, future work should investigate other electrode materials with larger overpotentials towards HER, such as copper. (See also Subsection 2.3.)

5.3 IR experiments

The occurrence of mass transport limited CO-bulk oxidation (Figure 30) and variable peaks from dissolved CO_2 (2300-2400 cm^{-1}) trapped in the thin electrolyte layer (Figure 31) showed that the electrolyte layer was too thick when a Parafilm gasket was used. But even without the Parafilm no CO related peaks, i.e. in the wavenumber range 2050-2100 cm^{-1}, were observed in the corresponding IR spectra at 45 $^\circ$ set incident angle, only variable peaks from dissolved CO_2 and in the wavenumber region related to adsorbed (bi-)sulfate [7], see Figure 31.

[1] Reaction (9) is a simplification of the hydrogen evolution reaction (HER).

The set incident angle of 53 degrees giving the maximal signal intensity was found by sweeping the set incident angle without electrolyte, i.e. with the crystal open to the atmosphere. The effective incident angle depend on the refraction indexes of the media in the beam path. So the set incident angle giving maximum signal intensity with electrolyte present may differ from 53 degrees. Less force was used when pressing down the electrode for the spectra shown in Figure 32 which show clear peaks in the CO bands region. The degree of pressing of the electrode against the crystal may affect the obtained spectra as written by the Moon et al. [25]. However, there are still some issues to be solved before good spectra can be obtained, see also Section 7.

The signal amplitude should exceed 5000 to obtain good spectra [36]. It turned out that ZnSe was incompatible with the electrolyte used in this work, because acidic solutions (pH $<$ 5) may etch the ZnSe crystal during prolonged exposure while strong acids may generate toxic hydrogen selenide [37, 38]. Etching of the crystal made it less transparent to infrared radiation, thus the observed degradation in signal amplitude.

The electrochemical procedures during IR scanning utilized the sequence function within Gamry Framework. It is uncertain whether the potential goes to open circuit between sequential steps. However, the open circuit potential with full CO coverage was measured to about 0.2-0.3 V and slowly rising, implying that minimal adsorbed CO were lost during short moments at OCP in saturated electrolyte.

6 Conclusion

Four alcohols and four carboxylic acids, namely methanol, ethanol, 1-propanol, 1-butanol, formic acid, acetic acid, propionic acid and butyric acid were studied in this masters thesis by electrochemical means with the aim of demonstrating any electrochemical reduction of carboxylic acids.

In general, oxidation of the alcohols happened more readily than oxidation of the acids (hence peak current density was significantly higher) which contained at least one C-C bond, most likely due to the simple dehydrogenation of the alcohol hydrogen leading to formation of aldehyde through the transfer of 2 electrons. At more positive potentials a distinct second oxidation peak was observed in the positive going sweep voltammetry experiment and is due to transfer of 2 more electrons yielding formation of the corresponding carboxylic acid. Due to the lack of a C-C bond, oxidation of methanol and formic acid, behaved significantly different than the other molecules used in this work. Rather quick formation of CO(ads) occur that will be oxidized to CO_2 at potentials in the oxide region. However, the peak potentials seems to be more dictated by the formation of an oxygen donating species (oxide) at the surface and its kinetics than the chemical compound and its reactivity (depends on the competition for active sites between the adsorption processes).

Looking closer at the lower potential end of the voltammetry experiments (H_{UPD} region), a dissimilarity was observed in particular between the base electrolyte and high concentration of longer chained acids (propionic and butyric acid). Furthermore, long-term experiments of holding a constant potential in the H_{UPD}/HER region gave rise to a new oxidation peak in the voltammogram, as well as a small reduction peak at about the same potential (0.5 V). This new characteristic may indicate the possible existence of a slow process in this low potential region. With continuous potential cycling, the oxidation and reduction pairs quickly ceased to exist, suggesting production of very small amounts. On the other hand, short term experiments gave no indications of production of anything other than hydrogen in the region. In most cases a slightly less negative current density was observed, probably due to some sort of blocking of the active sites by carbonaceous species.

The existence of an enhanced reduction current in the H_{UPD} region called for methods to detect adsorbed intermediates at the surface and soluble byproducts. A setup for external reflection mode ATR-FTIR spectroscopy was employed in this work. This system has not been used for electrochemical measurements and a conventional glass cell was designed and manufactured to render possible electrochemical measurements simultaneously with FTIR spectroscopy. In this project oxidation of CO was used to justify the setup and the glass cell. A small signal corresponding to adsorbed CO was indeed observed indicating that the setup is working as intended, although further work is needed to increase signal strength, improve quality and reproducibility.

We can not conclude or exclude whether the interesting current characteristics occurring in the hydrogen underpotential deposition region (especially for 1 M propionic and butyric acid), and during the long-term experiment for butyric acid is indeed electrochemical reduction. Further work concerning product analysis is highly desired.

7 Further work

- change electrocatalyst to e.g.. Cu
- change electrolyte to perchloric acid, less specific adsorption of anion
- Knowledge of the oxidation characteristics may be utilized for detection of reduction products with a rotating ring disk electrode.

References

[1] E. J. Cairns, A. D. Tevebaugh, and G. J. Holm. Thermodynamics of Hydrocarbon Fuel Cells. *J. Electrochem. Soc.*, 110(10):1025–1030, 1963.

[2] G. A. Olah, A. Goeppert, and G. K. Surya Prakash. *Beyond Oil and Gas: The Methanol Economy*. Wiley-VCH Verlag, 2006.

[3] http://www.butanol.com/biofuel.html. Bio-fuel. 20.06.2011.

[4] S. Atsumi, T. Hanai, and J. C. Liao. Non-fermentative pathways for synthesis of branched-chain higher alcohols as biofuels. *Nature*, 451:86–89, January 2008.

[5] F. A. Carey. *Organic Chemistry*, pages 144–147, 622–629, 794, 807–808. McGraw-Hill, 7th edition, 2008.

[6] Y HORI, H WAKEBE, T TSUKAMOTO, and O KOGA. Electrocatalytic Process of CO Selectivity in Electrochemical Reduction of CO2 at Metal-electrodes in Aqueous-media. *ELECTROCHIMICA ACTA*, 39(11-12):1833–1839, AUG 1994.

[7] M. Heinen, Y. X. Chen, Z. Jusys, and R. J. Behm. In situ ATR-FTIRS coupled with on-line DEMS under controlled mass transport conditions - A novel tool for electrocatalytic reaction studies. *ELECTROCHIMICA ACTA*, 52(18, Sp. Iss. SI):5634–5643, MAY 10 2007.

[8] M. Heinen, Z. Jusys, and R. J. Behm. *Handbook of Fuel Cells - Fundamentals, Technology and Applications*, volume 5: Advances in Electrocatalysis, Materials, Diagnostics and Durability, chapter 12, pages 183–214. John Wiley & Sons, Ltd., 2009.

[9] M. Heinen. *Electrooxidation of Small Organic Molecules, studied by Simultaneous in situ ATR-FTIRS and on-line Differential Electrochemical Mass Spectrometry*. PhD thesis, Ulm University, February 2010.

[10] M. Heinen, Y. X. Chen, Z. Jusys, and R. J. Behm. CO adsorption kinetics and adlayer build-up studied by combined ATR-FTIR spectroscopy and on-line DEMS under continuous flow conditions. *ELECTROCHIMICA ACTA*, 53(3):1279–1289, DEC 20 2007.

[11] S. Sun, M. Chojak Halseid, M. Heinen, Z. Jusys, and R. J. Behm. Ethanol electrooxidation on a carbon-supported Pt catalyst at elevated temperature and pressure: A high-temperature/high-pressure DEMS study. *JOURNAL OF POWER SOURCES*, 190(1, Sp. Iss. SI):2–13, MAY 1 2009.

[12] K. Kunimatsu, H. Hanawa, H. Uchida, and M. Watanabe. Role of adsorbed species in methanol oxidation on Pt studied by ATR-FTIRAS combined with linear potential sweep voltammetry. *JOURNAL OF ELECTROANALYTICAL CHEMISTRY*, 632(1-2):109–119, JUL 1 2009.

[13] F. Seland. TMT6 Oxidation of CO and small organic molecules. September 2010.

[14] F. Seland and B. T. Børresen. Project description: Electrochemical reduction of carboxylic acids. March 2010.

[15] *Handbook of Chemistry & Physics*, chapter 5: Thermochemistry, Electrochemistry, and Kinetics, pages 18–27. CRCnetBASE, http://www.hbcpnetbase.com, 91st edition, 2010-2011. 12.09.2010.

[16] Y. Hori, O. Koga, H. Yamazaki, and T. Matsuo. Infrared spectroscopy of adsorbed CO and intermediate species in electrochemical reduction of CO2 to hydrocarbons on a Cu electrode. *Electrochim. Acta*, 40(16):2617–2622, 1995.

[17] J. Lipkowski and P. N. Ross. *Electrocatalysis*. Wiley-VCH, New York, 1998.

[18] Y. Hori. *Electrochemical CO2 Reduction on Metal Electrodes*, pages 89–189. Number 42 in Modern Aspects of Electrochemistry. Springer, New York, 2008.

[19] F. Seland. TMT6 Fuel cells etc. September 2010.

[20] C. H. Hamann, A. Hamnett, and W. Vielstich. *Electrochemistry*, pages 260–272. Wiley-VCH Verlag, 2nd edition, 2007.

[21] D. A. Harrington. Simulation of anodic Pt oxide growth. *J. Electroanal. Chem.*, 420(1-2):101–109, 1997.

[22] http://www.gamry.com/Newsletter/2005Feb/RDE_Impedance.htm. Electrochemical Impedance at a Rotated Disk Electrode. 20.12.2010.

[23] M. Ystenes. Personal communication. Trondheim, June 2011.

[24] Bruker Optik GmbH. *OPUS Reference Manual*, 2002.

[25] SM Moon, C Bock, and B MacDougall. Setup, sensitivity and application of thin electrolyte layer ATR-FTIR spectroscopy. *JOURNAL OF ELECTROANALYTICAL CHEMISTRY*, 568(1-2):225–233, JUL 1 2004.

[26] F. Seland, R. Tunold, and D. A. Harrington. Impedance study of methanol oxidation on platinum electrodes. *ELECTROCHIMICA ACTA*, 51(18):3827–3840, MAY 5 2006.

[27] T. Iwasita. *Handbook of Fuel Cells - Fundamentals, Technology and Applications*, volume 2: Electrocatalysis, page 603. Wiley, Chichester, 2003.

[28] T Iwasita. Electrocatalysis of methanol oxidation. *ELECTROCHIMICA ACTA*, 47(22-23):3663–3674, AUG 30 2002.

[29] JM Leger. Mechanistic aspects of methanol oxidation on platinum-based electrocatalysts. *JOURNAL OF APPLIED ELECTROCHEMISTRY*, 31(7):767–771, 2001.

[30] S Wasmus and A Kuver. Methanol oxidation and direct methanol fuel cells: a selective review. *JOURNAL OF ELECTROANALYTICAL CHEMISTRY*, 461(1-2):14–31, JAN 29 1999.

[31] P Waszczuk, GQ Lu, A Wieckowski, C Lu, C Rice, and RI Masel. UHV and electrochemical studies of CO and methanol adsorbed at platinum/ruthenium surfaces, and reference to fuel cell catalysis. *ELECTROCHIMICA ACTA*, 47(22-23):3637–3652, AUG 30 2002.

[32] NH Li, SG Sun, and SP Chen. Studies on the role of oxidation states of the platinum surface in electrocatalytic oxidation of small primary alcohols. *JOURNAL OF ELECTROANALYTICAL CHEMISTRY*, 430(1-2):57–67, JUN 30 1997.

[33] R. Brateng. Electrooxidation of methanol and ethanol. Technical report, Department of Materials Science and Engineering and NTNU, 2004-2005.

[34] S.-G. Sun. *Electrocatalysis*, chapter 6, pages 243–290. Wiley-VCH, New York, 1998.

[35] F. Seland, R. Tunold, and D. A. Harrington. Impedance study of formic acid oxidation on platinum electrodes. *ELECTROCHIMICA ACTA*, 53(23, Sp. Iss. SI):6851–6864, OCT 1 2008.

[36] M. Sletnes. Personal communication. Trondheim, Spring 2011.

[37] http://www.piketech.com/technical/crystal-selection ATR.html. ATR CRYSTAL SELECTION. 10.05.2011.

[38] http://www.piketech.com/technical/faq.html. FREQUENTLY ASKED QUESTIONS. 16.05.2011.

[39] F. Seland. Personal communication. Trondheim, Spring 2010-2011.

[40] Frode Seland, Reidar Tunold, and David A. Harrington. Activating and deactivating mass transport effects in methanol and formic acid oxidation on platinum electrodes. *ELECTROCHIMICA ACTA*, 55(9):3384–3391, MAR 30 2010.

A Calculation of standard reduction potentials

Standard reduction potentials were calculated from thermodynamic data retrieved from CRC Handbook of Chemistry and Physics 91th ed., Section 5 [15].

The standard Gibb's free energy of formation was calculated from the standard enthalpy and entropy of formation at 298.15 K and standard conditions whenever it wasn't given directly.

$$\Delta_f G^o = \Delta_f H^o - T\Delta_f S^o$$

The standard Gibb's free energy of reaction was then calculated according to:

$$\Delta_{rx} G^o = \sum \Delta_f G^o(products) - \sum \Delta_f G^o(reactants)$$

Then standard reduction potential was calculated from:

$$E^o = \frac{-\Delta_{rx} G^o}{nF}$$

The resulting values for the standard reduction potentials are presented in Table 8.

Table 8: Standard reduction potentials calculated from thermodynamic data retrieved from ref. [15].

Theoretical cathodic half-reaction	$\Delta_{rx}G^o$ [kJmol^{-1}]	E^o [V vs. SHE]
$HCOOH + 4H^+ + 4e^- \rightarrow CH_3OH + H_2O$	-42.3	0.110
$CH_3COOH + 4H^+ + 4e^- \rightarrow CH_3CH_2OH + H_2O$	-13.0	0.034
$CH_3CH_2COOH + 4H^+ + 4e^- \rightarrow CH_3(CH_2)_2OH + H_2O$	-29.8	0.077
$CH_3(CH_2)_2COOH + 4H^+ + 4e^- \rightarrow CH_3(CH_2)_3OH + H_2O$	-31.7	0.082
$CH_3(CH_2)_2COOH + 2H^+ + 2e^- \rightarrow CH_3(CH_2)_2CHO + H_2O$	50.2	-0.260
$CH_3(CH_2)_2CHO + 2H^+ + 2e^- \rightarrow CH_3(CH_2)_3OH$	-81.9	0.424
$2H^+ + 2e^- \rightarrow H_2(g)$	-	0

B Estimation of active surface area

For the experimental determination of a true platinum surface via hydrogen adsorption by a cyclic voltammogram, the assumption that each platinum atom adsorbs one hydrogen atom is made [20]. The charge in the underpotential adsorption peaks of hydrogen on Pt were used for estimating the active surface area. This was assessed from a cyclic voltammogram at 100 mV/s as shown in Figure 34. A horizontal line was constructed as an approximate correction for the double-layer charging, and the initiation of H_2-evolution was omitted. The area under the curve, i.e. the charge, was found by utilizing the integration function within Echem Analyst. The integrated charge was then divided by the hydrogen capacity, which was taken to be 220 $\mu C/cm^2$ for polycrystalline platinum as used by Conway [39]. The active surface area was calculated before adding each organic species. There was little variation observed in the calculated active surface area, for the smooth Pt RDE.

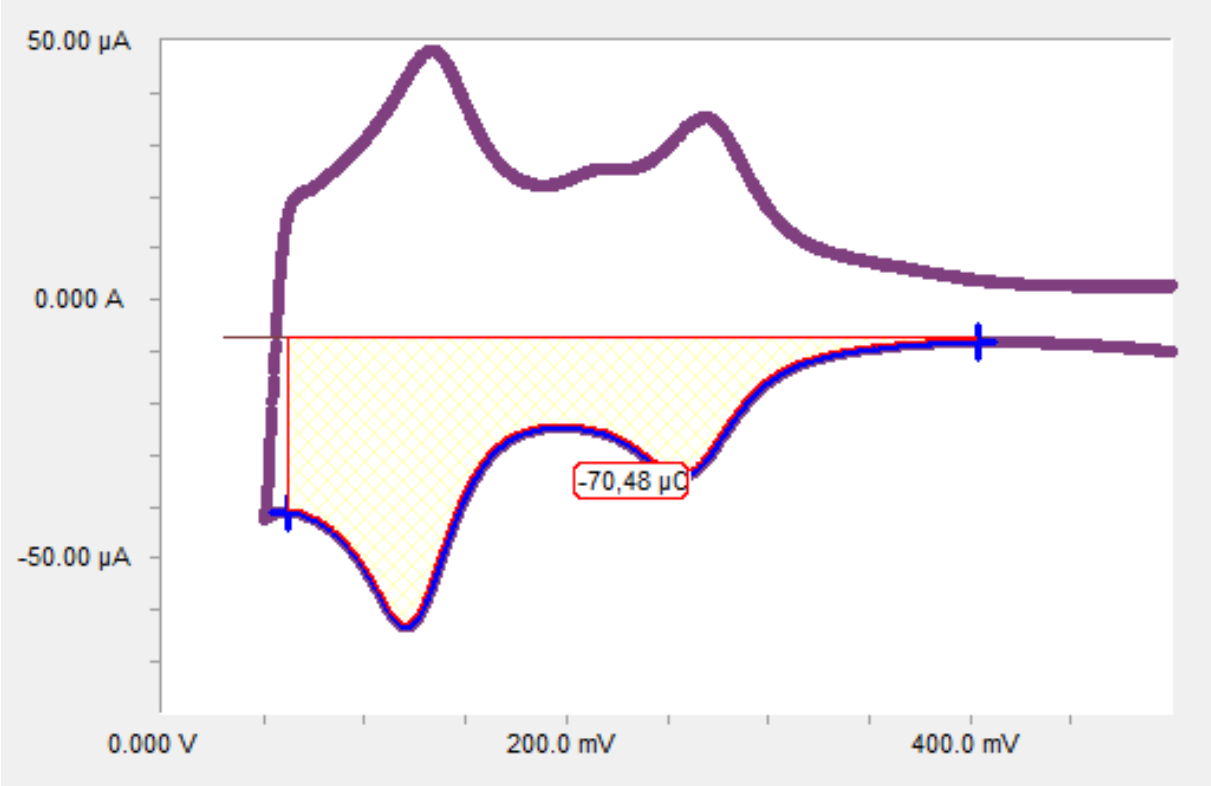

Figure 34: The section of a cyclic voltammogram of Pt in base electrolyte at 100 mV/s used for integration of charge, in Echem Analyst, for the calculation of active surface area.

C Additional electrochemical measurements

C.1 Oxidation processes

C.1.1 Sweep rate, normalized with respect to charge

Figures 35-38 show CVs of various sweep rates in 0.01 M and 1 M of alcohols and 0.01 M and 1 M of carboxylic acids, respectively, where the current density is normalized to 100 mV/s with respect to charge. It is not strictly correct to discuss normalized voltammograms for processes under mixed control. However, the changes in the hydrogen region caused by carbonaceous species become more clear when the current density is normalized. The peak current densities decrease with increasing sweep rate due to less time for reactions to occur. Methanol with its single carbon, stand out from the other alcohols, because the electrode surface get fully blocked by CO at low potentials. The H_{UPD} region is less affected by sweep rate in ethanol, propanol and butanol. In 0.01 M methanol (Figure 35a) full blocking is not achieved for the fastest sweep rates, hence more pronounced hydrogen adsorption and desorption peaks are observed. Less CO blockage during the reverse sweep is due to less time for reactions to occur at high sweep rate, meaning less adsorbate is formed. The separation of the anodic peaks in 0.01 M (Figure 35) and 1 M (Figure 36) of ethanol, propanol and butanol become more pronounced at lower sweep rates.

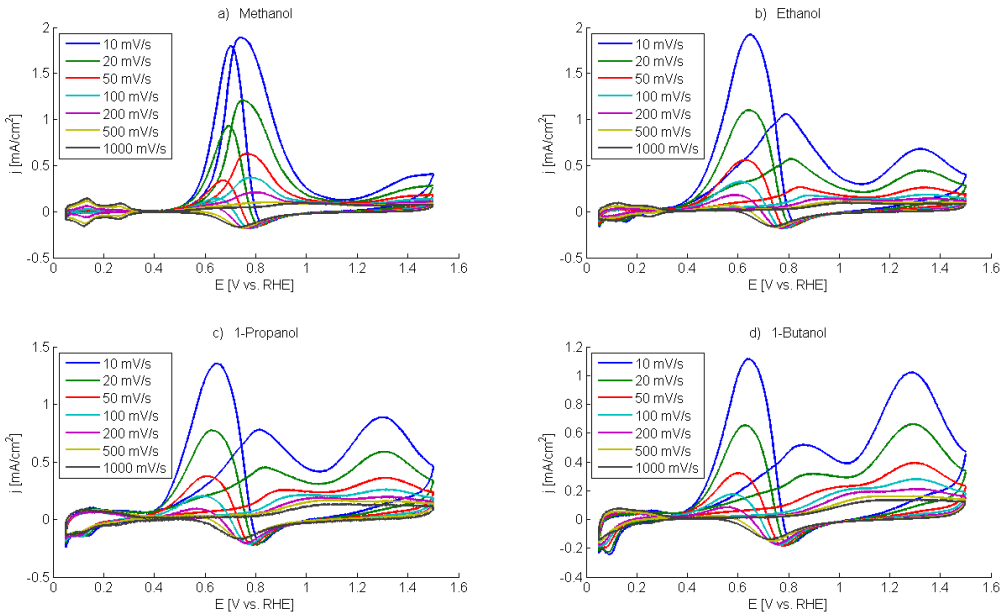

Figure 35: Effect of sweep rate in the presence of 0.01 M of (a) methanol, (b) ethanol, (c) 1-propanol, (d) 1-butanol, normalized to 100 mV/s.

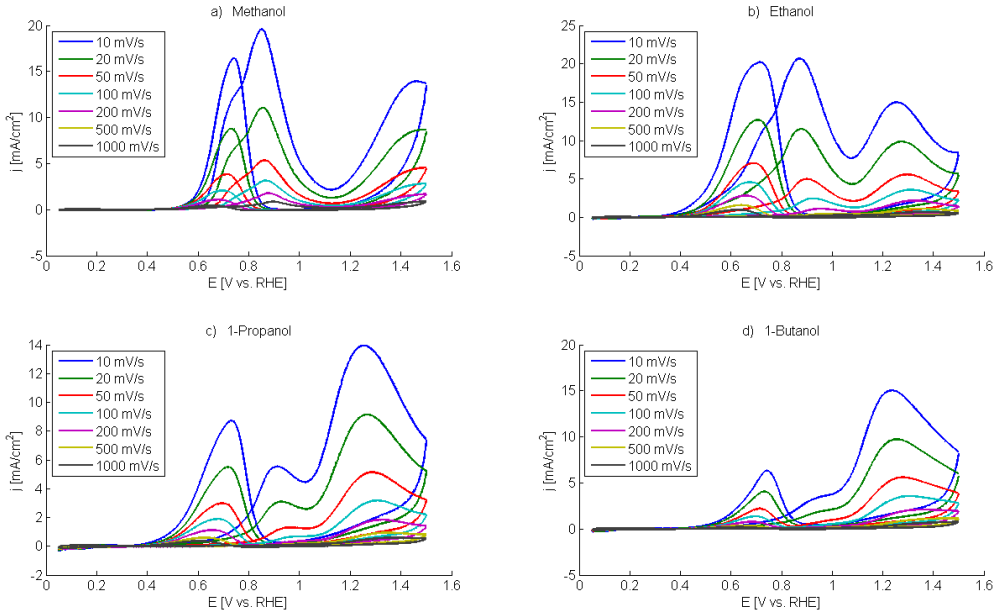

Figure 36: Effect of sweep rate in the presence of 1 M of (a) methanol, (b) ethanol, (c) 1-propanol, (d) 1-butanol, normalized to 100 mV/s.

It can be seen from Figure 37 and 38 that the cathodic current response below 150 mV in the reverse sweep is most pronounced for the lowest sweep rates, when normalization is done, indicating that this process is influenced by mass transport. The oxidation peak is also more pronounced at lower sweep rates.

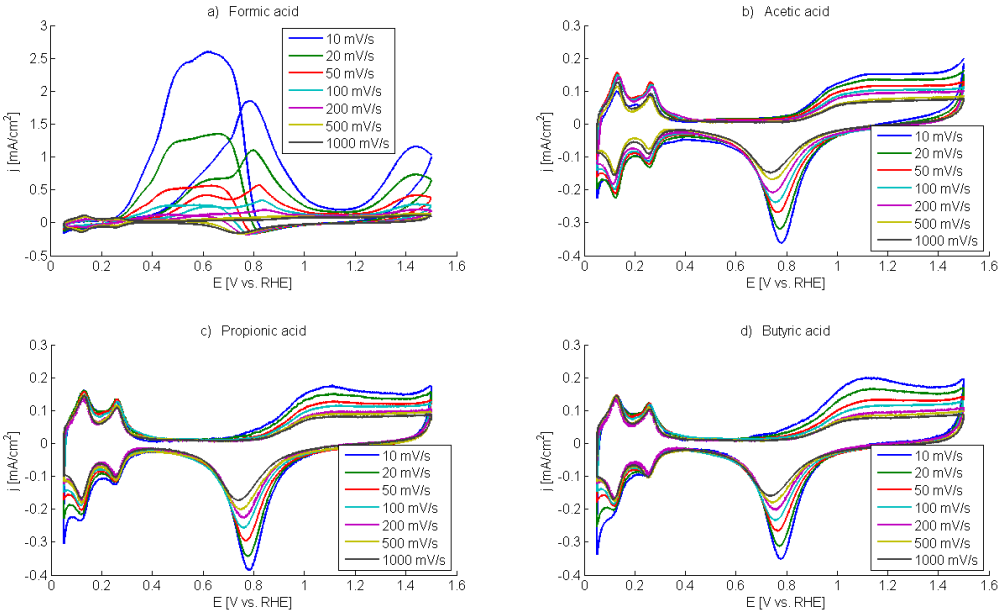

Figure 37: Effect of sweep rate in the presence of 0.01 M of (a) formic acid, (b) acetic acid, (c) propionic acid and (d) butyric acid, normalized to 100 mV/s.

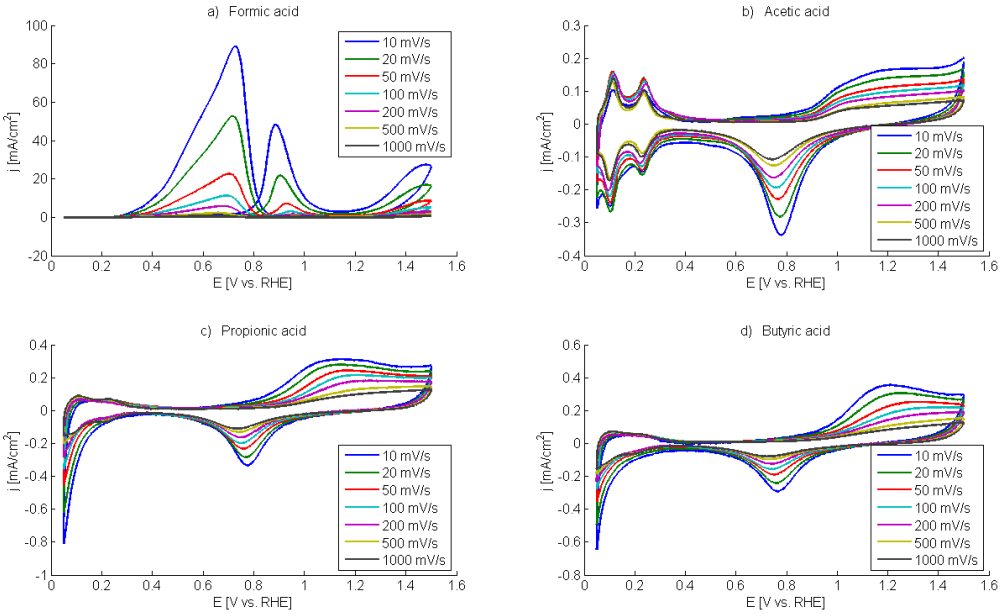

Figure 38: Effect of sweep rate in the presence of 1 M of (a) formic acid, (b) acetic acid, (c) propionic acid and (d) butyric acid, normalized to 100 mV/s.

C.1.2 Effect of positive turn-round potential (1-propanol)

Voltammograms of 0.01 and 1 M propanol at 100 mV/s with the positive turn-round potential increased by increments of 0.1 V are shown in Figure 39. The imposed potential-time function giving rise to the plotted voltammograms is also included. It is evident from this figure that moving the positive turn-round potential to more positive potentials lead to an increase in the quantity of surface oxide formed and consequently in the subsequent reduction peak. The oxide reduction peak is absent when the positive turn-round potential is negative to 0.9 V, below which no Pt oxide formation occur. Clearly, the higher the upper reversal, the longer you have to wait for oxidation in the reverse sweep to commence, indicating again the importance of reducing enough oxide to get the oxidation lifted. An increase in the cathodic current response in the hydrogen region with increasing upper potential limit is observed for both concentrations. However, the change when increasing the positive turn-round potential to 1 V is largest in 0.01 M propanol.

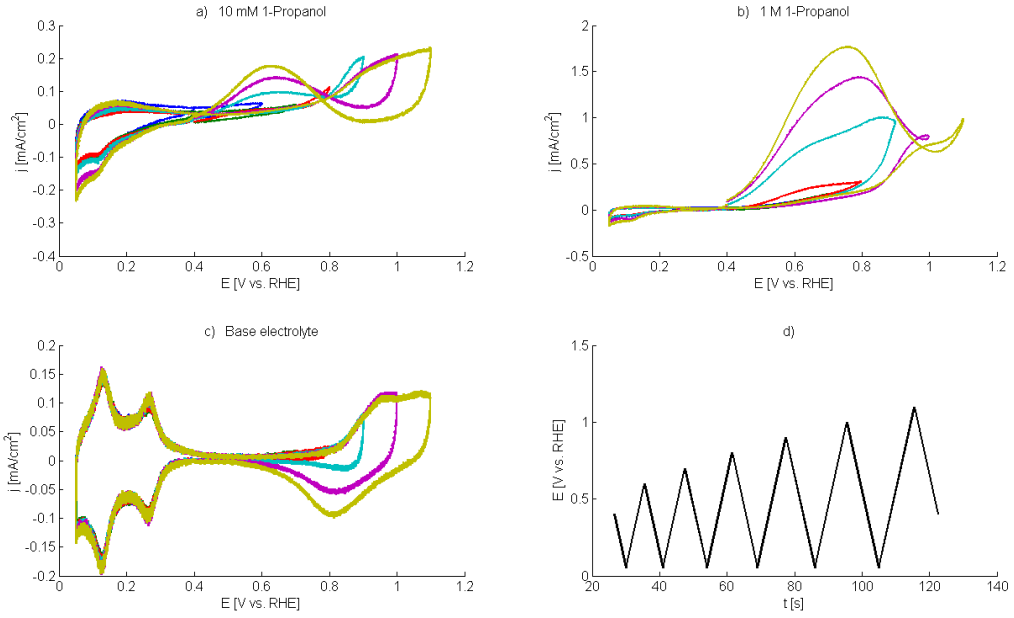

Figure 39: Voltammograms at 100 mV/s with the positive turn-round potential increased by 100 mV, from 0.6 V to 1.1 V, for each cycle in (a) 0.01 M and (b) 1 M of 1-propanol, and in (c) the base electrolyte, (d) the imposed triangular wave giving these results.

C.1.3 Rotation

Cyclic voltammograms of various number of rotation rates in 0.01 and 1 M of some of the alcohols at 10 and 100 mV/s, respectively, are presented in Figures 40-43. The mass transport effect is most pronounced in the reverse sweep peak for both concentrations at 10 mV/s, see Figure 40and 41.

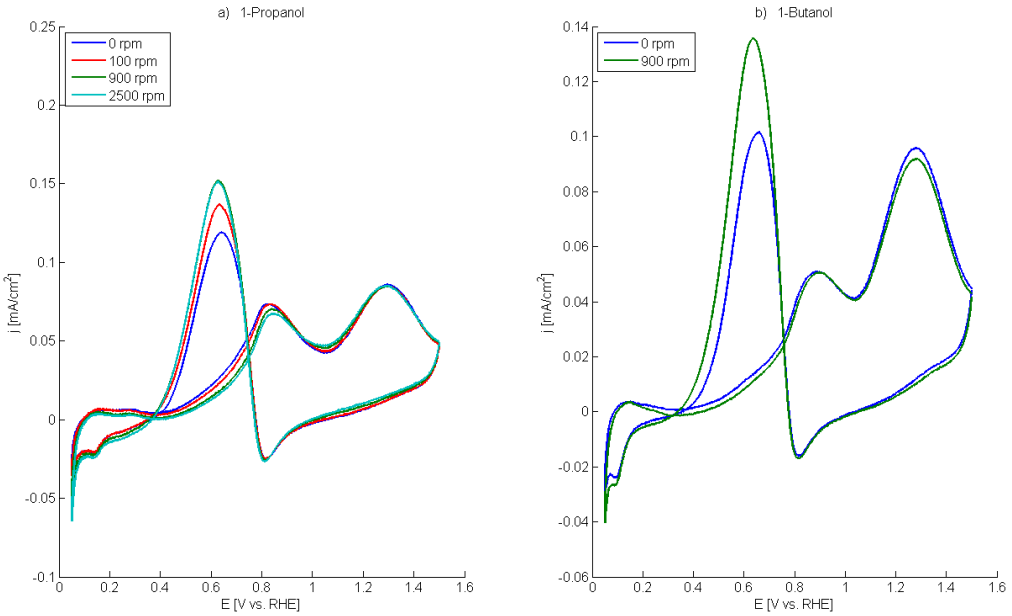

Figure 40: Cyclic voltammograms of Pt at various rotation rates at 10 mV/s in 0.01 M of (a) 1-propanol, (b) 1-butanol.

An additional shoulder prior to the first peak in the positive going sweep is observed for 0.01 M of propanol and butanol at 100 mV/s in Figure 42. Fast sweep rate prevent surface equilibrium from being maintained, creating an additional surface condition [35]. A delicate balance between rotation and sweep rate affect the observed current response, most likely again due to competition between adsorbed species (i.e. water and alcohol), or between adsorption and production of solved species. When no rotation was applied, the (over)potential was the only driving force, and H_2O was adsorbed at all (most) of the active sites. Rotation facilitated the mass transport of alcohol to the electrode surface by decreasing the diffusion layer thickness. Thus both mass transport and potential became driving forces. This rendered the adsorption reaction of alcohol more competitive. So the ratio of adsorbed alcohol over H_2O(ads) increased with rotation rate, until the point where practically all the active sites were occupied by alcohol. The overall oxidation reaction could be as follows:

$$\mathrm{ROH(ads)} + \mathrm{H_2O(ads)} \rightarrow \mathrm{ROOH} + 4\,\mathrm{H^+} + 4\,\mathrm{e^-}$$

or

$$\mathrm{ROH(ads) + H_2O(ads) \rightarrow RHO + 2\,H^+ + 2\,e^-}$$

giving carboxylic acid or aldehyde as final oxidation product, cf. Brateng's work on ethanol [33].

The potential driving force got so big from about 1.0 V and upwards, that mass transport became unimportant at this sweep rate. The effect of rotation on the current response is less in 1 M at 100 mV/s, Figure 43 which we do not want to focus on in this work.

Cyclic voltammograms of various number of rotation rates in 0.01 and 1 M of carboxylic acids at 10 and 100 mV/s, respectively, are presented in Figures 44-47. Formic acid stand out from the other acids, and display a decrease in anodic peak current density, in both forward and reverse sweep direction (Figure 45), as described in literature [40]. High rate of rotation, and low sweep rate, make the oxidation peak more pronounced for propionic and butyric acid, see Figure 44. It is apparent from Figure 44b-d that the cathodic current response below 150 mV in the reverse sweep at 10 mV/s increase with rotation rate. The increase is less in 1 M, see Figure 45, since it's already high without rotation at this concentration. This implies that the occurring reduction/adsorption process is influenced by mass transport. The effect of rotation is less for the higher sweep rate, especially for 1 M concentration of acids, see Figure 46 and 47. Hence, it rely on concentration. However, it was not affected by sweep rate. This indicate that a chemical step may be involved.

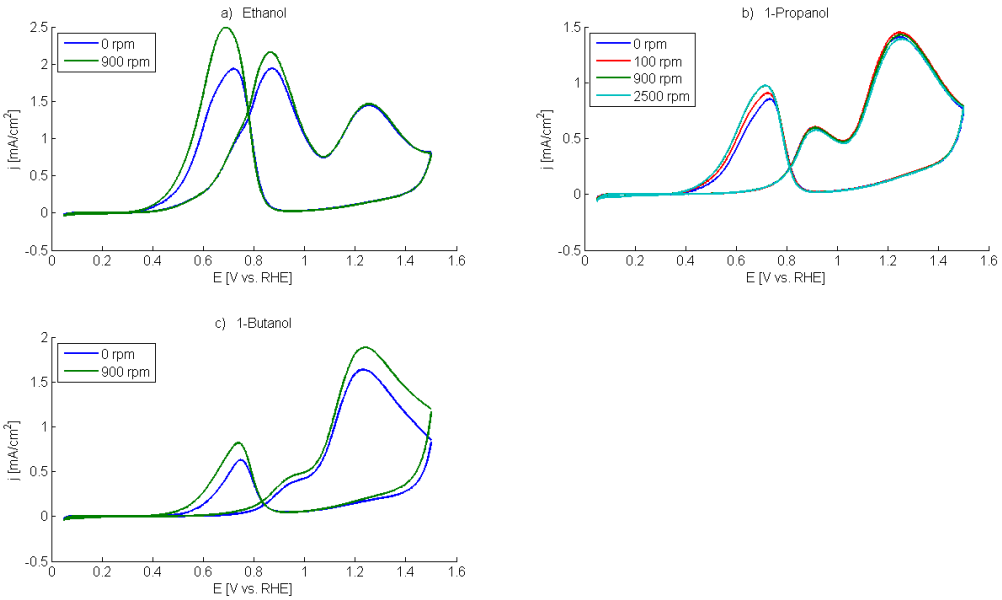

Figure 41: Cyclic voltammograms of Pt at various rotation rates at 10 mV/s in 1 M of (a) ethanol, (b) 1-propanol, (c) 1-butanol.

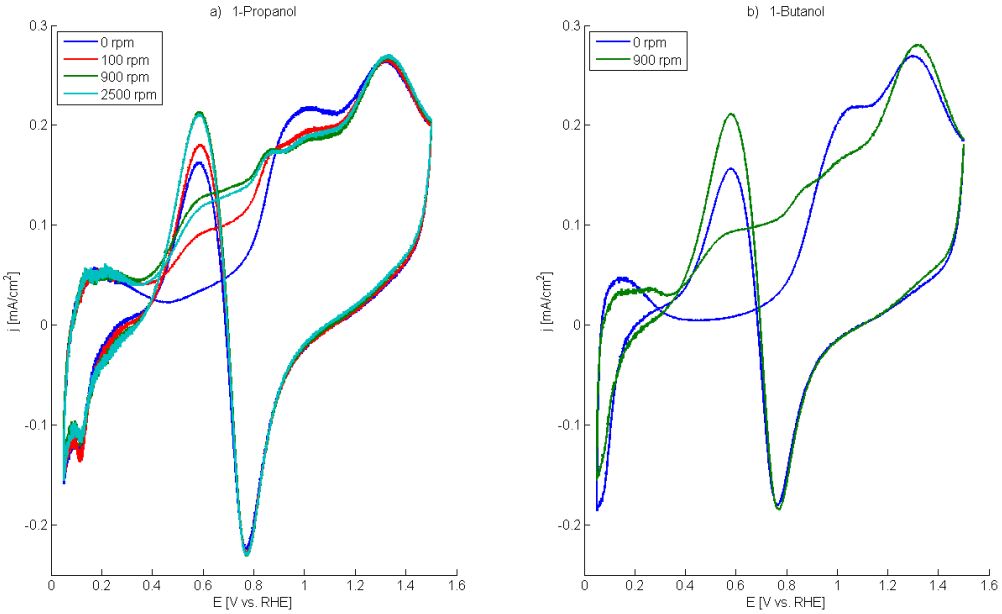

Figure 42: Cyclic voltammograms of Pt at various rotation rates at 100 mV/s in 0.01 M of (a) 1-propanol, (b) 1-butanol.

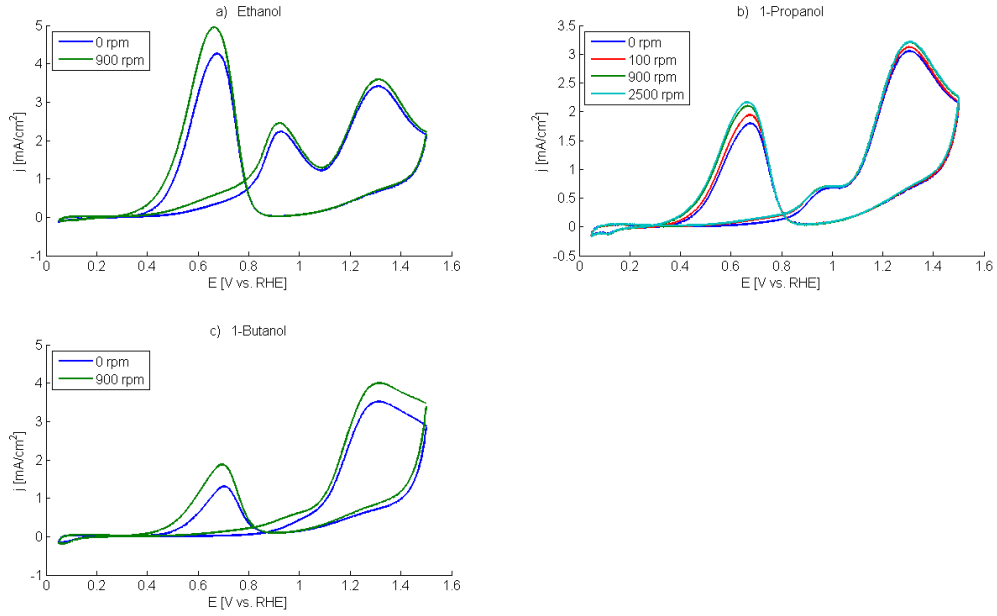

Figure 43: Cyclic voltammograms of Pt at various rotation rates at 100 mV/s in 1 M of (a) ethanol, (b) 1-propanol, (c) 1-butanol.

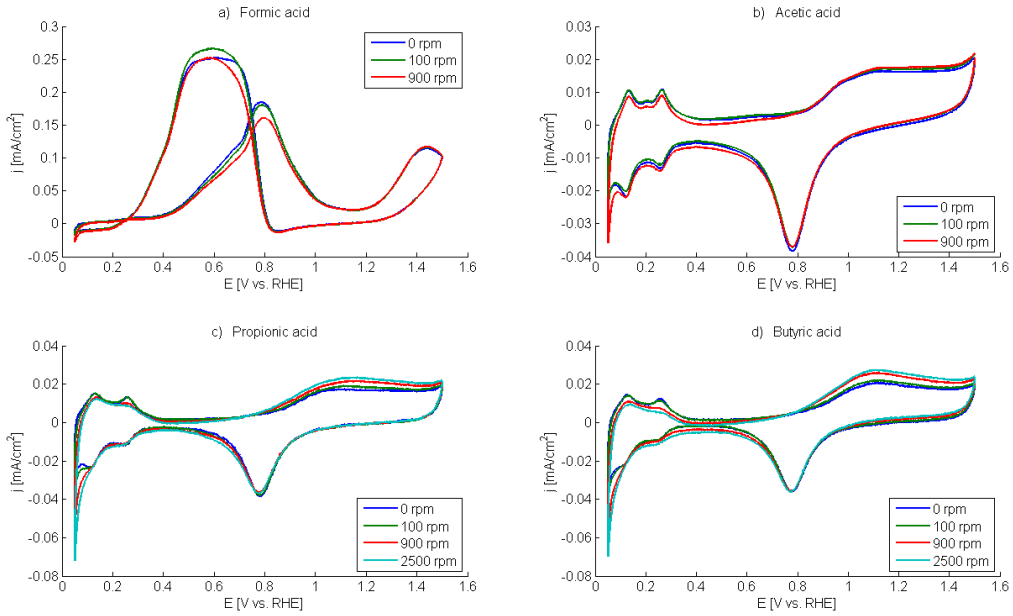

Figure 44: Cyclic voltammograms of Pt at various rotation rates at 10 mV/s in 0.01 M of (a) formic acid, (b) acetic acid, (c) propionic acid and (d) butyric acid with a negative turn-round potential of 50 mV.

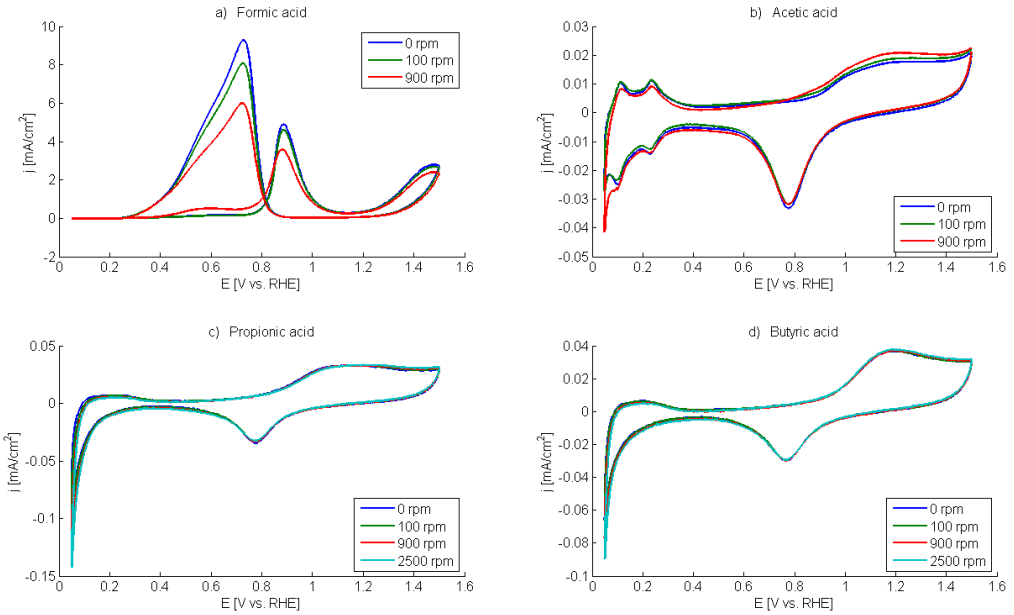

Figure 45: Cyclic voltammograms of Pt at various rotation rates at 10 mV/s in 1 M of (a) formic acid, (b) acetic acid, (c) propionic acid and (d) butyric acid with a negative turn-round potential of 50 mV.

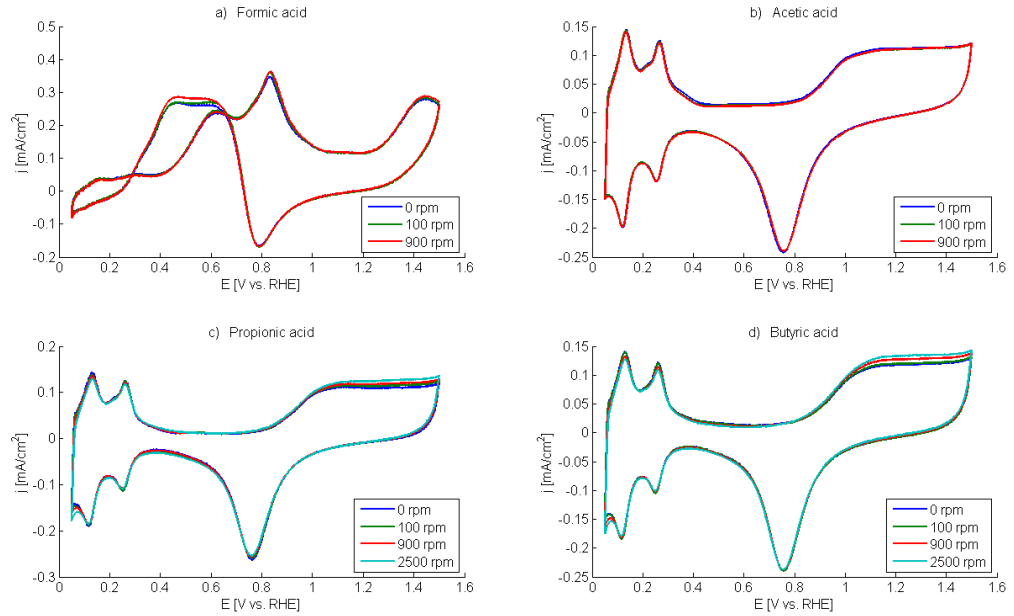

Figure 46: Cyclic voltammograms of Pt at various rotation rates at 100 mV/s in 0.01 M of (a) formic acid, (b) acetic acid, (c) propionic acid and (d) butyric acid with a negative turn-round potential of 50 mV.

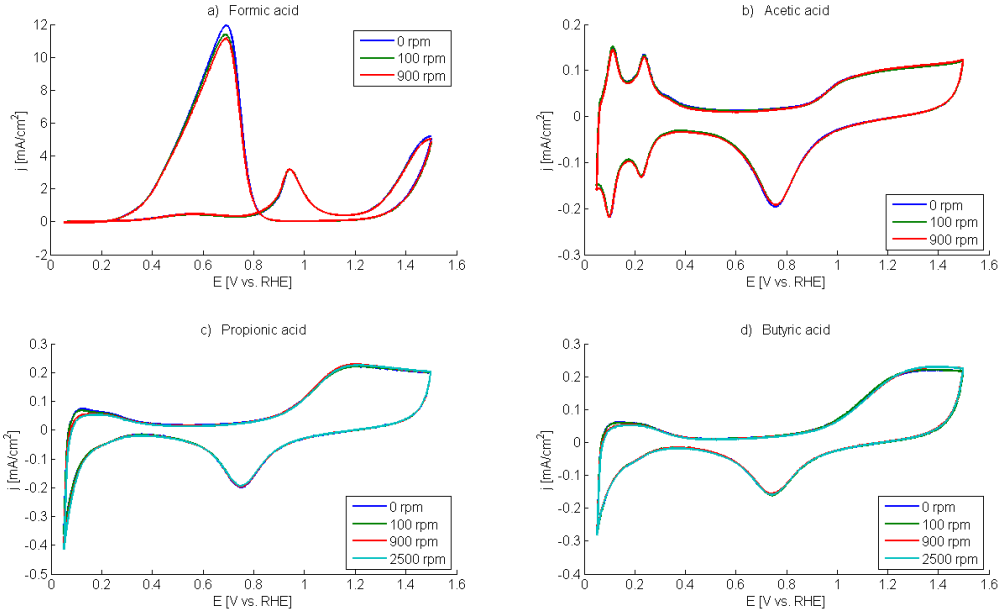

Figure 47: Cyclic voltammograms of Pt at various rotation rates at 100 mV/s in 1 M of (a) formic acid, (b) acetic acid, (c) propionic acid and (d) butyric acid with a negative turn-round potential of 50 mV.

C.2 Reduction processes

Rotation had no extra effect on the anodic part of the CVs in Figure 48 when going to more negative potentials than 50 mV. However, the hydrogen evolution current density is slightly less in propionic and butyric acid compared with base electrolyte current response. The increase in cathodic current density with increasing rotation rate seen in Figure 49 is due to the better transport of evolved H_2(g) away from the surface. The current density is so similar in the base electrolyte.

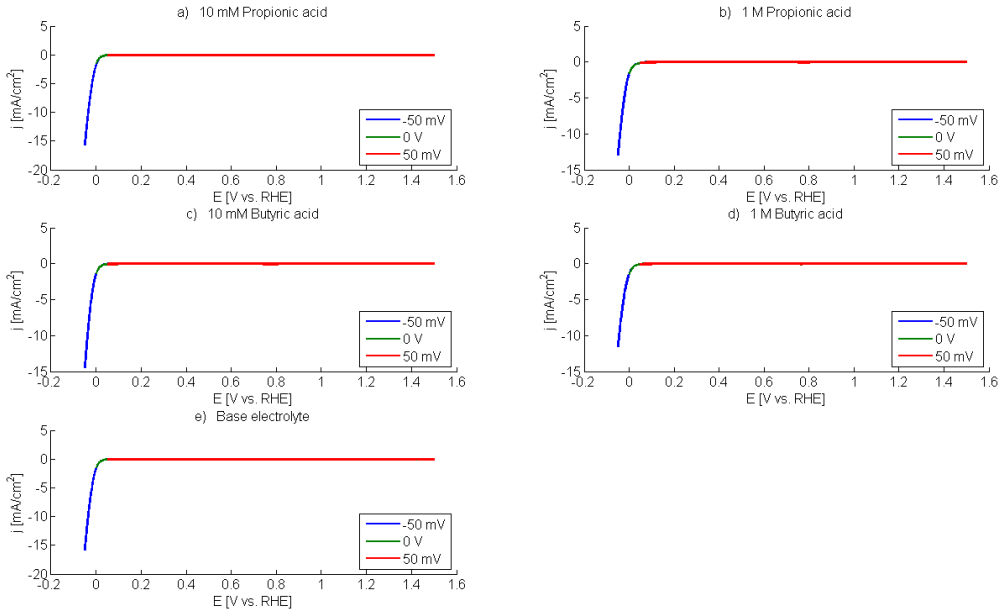

Figure 48: Cyclic voltammograms with various negative turn-round potentials at 10 mV/s and 2500 rpm rotation in (a) 0.01 M and (b) 1 M of propionic acid, (c) 0.01 M and (d) 1 M of butyric acid, and in (e) the base electrolyte.

No significant effect of rotation was observed in the linear voltammograms after holding at 50 mV for 300 s, shown in Figure 50.

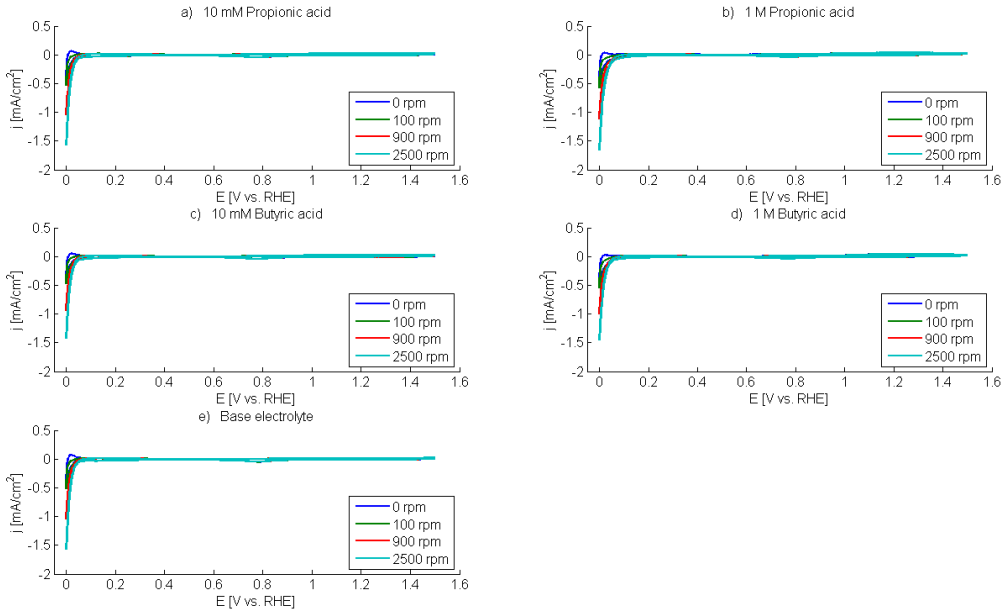

Figure 49: Cyclic voltammograms of Pt with a negative turn-round potential of 0 V at various rotation rates at 10 mV/s in (a) 0.01 M and (b) 1 M of propionic acid, (c) 0.01 M and (d) 1 M of butyric acid, and in (e) the base electrolyte.

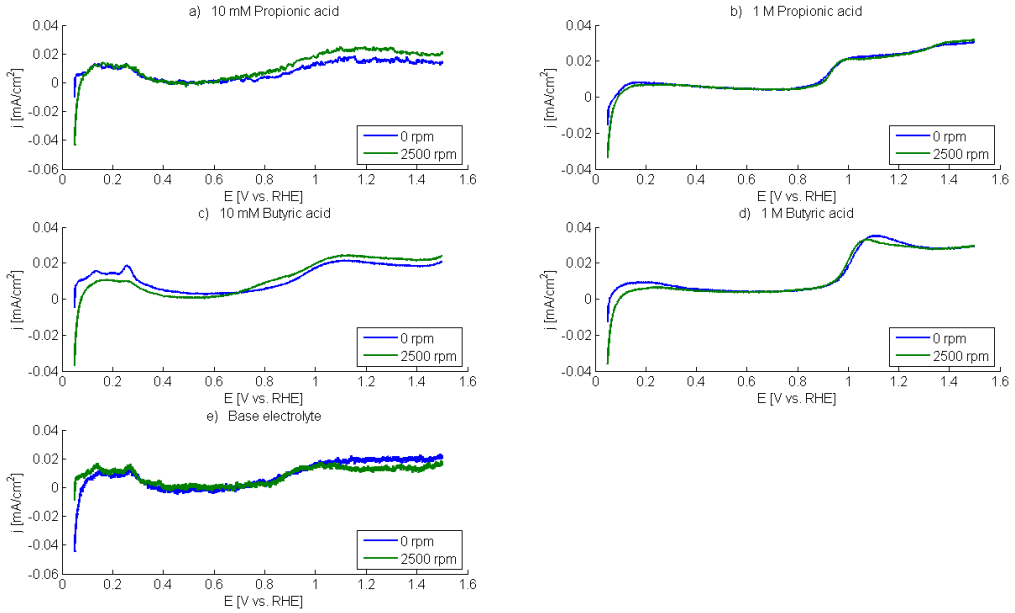

Figure 50: Linear voltammograms at 10 mV/s following 300 s at 50 mV in (a) 0.01 M and (b) 1 M of propionic acid, (c) 0.01 M and (d) 1 M of butyric acid, and in (e) the base electrolyte.